

CONFIDENTIAL

Copy
RM L50108

UNAVAILABLE

NACA RM L50108

NACA

RESEARCH MEMORANDUM

INVESTIGATION AT A MACH NUMBER OF 1.93 TO
DETERMINE LIFT, DRAG, PITCHING-MOMENT, AND AVERAGE DOWNWASH
CHARACTERISTICS FOR SEVERAL MISSILE CONFIGURATIONS HAVING
RECTANGULAR WINGS AND TAILS OF VARIOUS SPANS

By Carl E. Grigsby

Langley Aeronautical Laboratory
Langley Air Force Base, Va.

CLASSIFIED DOCUMENT

This document contains classified information affecting the National Defense of the United States within the meaning of the Espionage Act, USC 50-31 and 32. Its transmission or the revelation of its contents in any manner to an unauthorized person is prohibited by law.
Information so classified is to be limited only to persons in the military and naval services of the United States, appropriate civilian officers and employees of the Federal Government who have a legitimate interest therein, and to United States citizens of known loyalty and discretion who of necessity must be informed thereof.

**NATIONAL ADVISORY COMMITTEE
FOR AERONAUTICS**

WASHINGTON

October 19, 1950

CONFIDENTIAL

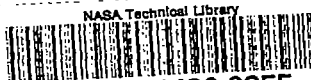
UNAVAILABLE

CLASSIFICATION CHANGED

UNCLASSIFIED UNAVAILABLE

To

Authority of *105-10-4-57* Date *10/19/50*



3 1176 01436 2355

NATIONAL ADVISORY COMMITTEE FOR AERONAUTICS

RESEARCH MEMORANDUM

INVESTIGATION AT A MACH NUMBER OF 1.93 TO
DETERMINE LIFT, DRAG, PITCHING-MOMENT, AND AVERAGE DOWNWASH
CHARACTERISTICS FOR SEVERAL MISSILE CONFIGURATIONS HAVING
RECTANGULAR WINGS AND TAILS OF VARIOUS SPANS

By Carl E. Grigsby

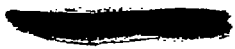
SUMMARY

An investigation has been made at a Mach number of 1.93 to determine lift, drag, pitching-moment, and average downwash characteristics of several missile configurations. Five configurations having rectangular wings and tails of various spans were tested; each of these configurations had two locations of the wing relative to the tail. The Reynolds number of the tests was 2.80×10^6 based on the body length and 0.19×10^6 based on the wing chord.

The experimental average downwash values showed agreement with a theoretical approximation only at small angles of attack. At higher angles of attack, distortion and displacement of the trailing vortex sheet produced large differences between experiment and theory. The experimental lift-curve slope of the wing in the presence of the body was compared with theoretical lift-curve slopes. The theoretical estimates were found to be inadequate at the lower aspect ratios with good agreement indicated at the high aspect ratios.

INTRODUCTION

The problem of satisfactory longitudinal stability at supersonic speeds for missiles has become of increasing importance. The use of low-aspect-ratio lifting and stabilizing surfaces has introduced major difficulties in missile design because of the complexity of wing downwash and interference effects. Although many data are available concerning longitudinal stability of specific missile configurations, it is difficult to obtain general information from these results because of the variety of configurations and the widely different test techniques.



As part of a general study of longitudinal-stability problems at supersonic speeds, an investigation of downwash effects on a configuration with a rectangular wing and tail was made in the Langley 9-inch supersonic tunnel and the results were reported in reference 1. Recent tests at supersonic speeds of two missile configurations, the MX-904 and the Rascal, (references 2, 3, and 4) have shown adverse stability changes at angles of attack around zero for the in-line configurations and at angles of attack of 6° to 8° for the so-called interdigitated configuration. Certain geometric properties appear common to these missiles; namely, low-aspect-ratio wings and tails of nearly equal span, and small ratios of wing span to body diameter.

An investigation of the in-line case to determine some effects of varying wing and tail aspect ratios and ratio of wing span to body diameter has been made in the Langley 9-inch supersonic tunnel and is reported here. Three-component measurements were made at a Mach number of 1.93 on a configuration with rectangular wing and tail over a range of angles of attack from 1° to 13° . For two longitudinal locations of the wing relative to the tail and for two tail incidence angles, tests were made with five combinations of wing and tail aspect ratios.

SYMBOLS

A	aspect ratio $\left(\frac{b^2}{S}\right)$
b	wing span
c	wing chord
S	wing area
d	body diameter
l	wing location - distance from leading edge of tail to leading edge of wing
x	center-of-gravity location - distance from center of gravity to rear of body
α	angle of attack
i_t	tail incidence angle
ϵ	average flow angle of tail, positive downward

M	Mach number
ρ	stream density
V	free-stream velocity
q	dynamic pressure $\left(\frac{1}{2}\rho V^2\right)$
C_L	lift coefficient $\left(\frac{\text{Lift}}{qS}\right)$
C_D	drag coefficient $\left(\frac{\text{Drag}}{qS}\right)$
C_m	pitching-moment coefficient $\left(\frac{\text{Moment about center of gravity}}{qSc}\right)$
C_{L_α}	lift-curve slope $\left(\frac{\partial C_L}{\partial \alpha}\right)$
$(C_{L_{\alpha_w}})_b$	incremental lift-curve slope of wing $(C_{L_{\alpha_{BW}}} - C_{L_{\alpha_B}})$
η_t	wing-wake parameter $\left(\left(\frac{\partial C_L}{\partial i_t}\right)_{bw} / \left(\frac{\partial C_L}{\partial i_t}\right)_b\right)$

Subscripts:

BWT	configuration of body, wing and tail
BW	configuration of body and wing
BT	configuration of body and tail
B	configuration of body
b	in presence of body
bw	in presence of body and wing
w	due to addition of wing
cg	refers to center of gravity

APPARATUS AND TESTS

Description of Tunnel

The Langley 9-inch supersonic tunnel is a closed-return, direct-drive type in which the pressure and humidity are controlled. The test Mach number is varied by means of interchangeable nozzle blocks forming a test section of approximately 9-inches square. Eleven fine-mesh, turbulence-damping screens are provided in the settling chamber ahead of the nozzles. During the tests the amount of water vapor in the tunnel air was kept at sufficiently low values so that the effects of condensation in the test section were negligible.

Description of Model and Tunnel Setup

A drawing of the model and support installation is shown in figure 1 and a photograph of the top view of the tunnel installation is shown in figure 2. The gap between the moveable windshield and the rear of the model shown in figure 2 is larger than the gap used during the tests. The diameter of the moveable windshield was slightly smaller than the rear of the model to prevent any scoop-off effects due to slight asymmetry between the rear of the model and the moveable windshield.

A drawing of the model is shown in figure 3 and the principal dimensions are given in table I. The model is the same one used for the tests of reference 1 except that different forward surfaces were used for the present tests. The wing and tail surfaces are 6-percent circular-arc sections with maximum thickness at 50 percent chord. The wing aspect ratio was varied in steps of 6.89, 5.64, 4.36, and 3.10 with the tail aspect ratio equal to 4.03. For the wing aspect ratio of 3.10, a configuration with the tail aspect ratio reduced to 2.95 was made. The different aspect ratios of both wing and tail were obtained by progressively shortening the spans of the surfaces.

Test Methods

Measurements of lift, drag, and pitching moment were made through an angle-of-attack range of 1° to 13° . As shown in figure 2, the moveable windshield was beveled to provide a symmetrical clearance between the rear of the body and the moveable windshield which was kept at 0.004 inch throughout the tests. An optical system employing a small mirror mounted in the rear of the body was used to measure angles of attack. This system gave true angles directly with no correction necessary for model sting deflection.

Although base-pressure measurements were not made, tests of several similar models in which the base pressure was measured have shown that the base pressure was equal to the pressure in the sting-shield-and-balance enclosing box and was constant over the base of the model, provided the gap between the moveable windshield and the rear of the body is less than 0.005 inch and provided the eccentricity between the moveable windshield and the rear of the model is small. Measurements of the pressure in the sting-shield-and-balance enclosing box were made and the drag results were corrected to the condition of base pressure equal to stream pressure.

Three-component measurements were made with self-balancing mechanical scales, and check measurements were made using an internal strain-gage balance similar to that used in reference 1. The check tests using the strain gages were made for only the B, BW-model 4, and BT-model 5 configurations, since these configurations had small lift forces and bracketed the extreme locations of the center of pressure.

Precision of Data

The precision of the data has been evaluated by estimating the uncertainties in each item involved in a given quantity and combining these errors by a method based on the theory of least squares.

The precision of the scale lift coefficient involves only the uncertainty of the mechanical scales, whereas the scale pitching-moment coefficient involves, in addition, the location of the moment reference. The scale drag coefficient contains the errors in the pressure-force correction to the drag in addition to the uncertainty of the mechanical scales. It is estimated that the maximum uncertainty in C_D from this pressure-force correction is about ± 0.0001 .

The final uncertainty in the strain-gage measurements involved only the random shifts in zero readings since there were observed no significant changes in calibration during the tests.

Angles of attack of the model could be read visually to an accuracy of $\pm 0.01^\circ$, whereas the model could be reset relative to the air stream and sidewalls upon each installation within $\pm 0.03^\circ$.

A summary table of precision estimates is as follows:

Lift coefficient, C_L :	
Scale	± 0.0003
Strain gage	± 0.0010
Pitching-moment coefficient, $C_m(\frac{l}{c} = 7.08)$:	
Scale	± 0.005
Strain gage	± 0.006
Pitching-moment coefficient, $C_m(\frac{l}{c} = 4.55)$:	
Scale	± 0.004
Strain gage	± 0.003
Drag coefficient, C_D (scale)	± 0.003
Angle of attack, α (initial)	± 0.03
Angle of attack, α (relative)	± 0.01
Tail incidence angle, i_t	± 0.03
Mach number, M	± 0.01

RESULTS AND DISCUSSION

The variations of lift, drag, and pitching moment with angle of attack for the BWT, BW, BT, and B configurations are shown in figures 4 and 5. All coefficients are based on the individual wing areas and the pitching-moment coefficients are referenced to a point one body diameter ahead of the aerodynamic center of the BWT configuration at 2° angle of attack. The results of strain-gage check tests, figures 4(a), 4(g), 4(i), and 5(e), indicate that the forces on the model sting and the model-sting support are negligible, and that the forces measured by the mechanical scales are the aerodynamic forces on the model. It should be recognized that although the results do not contain effects of the model sting, they do contain effects of the moveable windshield upon the flow over the rear of the body. Other tests of similar configurations have shown these effects to be small.

Lift and Drag Results

Lift.— The body lift-curve slope shows a considerable increase with increasing angle of attack. A similar increase in the BWT lift-curve slope is primarily the result of this increase in the body lift-curve slope. Other causes of the nonlinear BWT lift-curve slopes are the increasing lift-curve slope of the isolated wing and tail and the decrease in wing downwash with increasing angle of attack which will be

discussed subsequently. The lift curves for the BWT and BT configurations with the higher incidence angle show a smaller slope at the higher angles of attack than do the corresponding results for the configurations with the lower incidence angles. This smaller slope for the higher incidence angle results is probably due to decreasing lift-curve slope of the tail at higher absolute angles of attack.

A comparison with experimental results of several approximate theoretical methods of calculating the effect of body upwash upon the incremental lift-curve slope of rectangular wings is shown in figure 6. The experimental lift-curve slopes $(C_{L_{\alpha W}} - C_{L_{\alpha B}})$ were taken at about 2° angle of attack.

In the approximate theoretical methods for calculating the effects of body upwash, the flow about the body is assumed to be the flow about an infinite cylinder and the lift is summed by the strip method, that is, the lift is assumed proportional to the local angle of attack. If the lift in the tip section of the wing is 0.75 of the two-dimensional lift and if there is an angle of attack of 2α carried over the body, then it can be shown that the incremental lift-curve slope of the wing would be

$$(C_{L_{\alpha W}})_b = \frac{4}{\beta} \left[\frac{n+2}{n} - \frac{1}{2A\beta} - \frac{1}{2n^2} \left(\frac{2A\beta-3}{A\beta-2} \right) \right] \quad (1)$$

where $\beta = \sqrt{M^2 - 1}$ and n is the ratio of wing span to body diameter (b/d). If similar assumptions are made, except that an angle of α (unit lift) is carried over the body, then the lift-curve slope is equal to

$$(C_{L_{\alpha W}})_b = \frac{4}{\beta} \left[\frac{n+1}{n} - \frac{1}{2A\beta} - \frac{1}{2n^2} \left(\frac{2A\beta-3}{A\beta-2} \right) \right] \quad (2)$$

In reference 5, the lift of a wing in the presence of a body is expressed as the wing-alone lift times an effectiveness factor. This effectiveness factor is obtained by integration over the entire wing span of the upwash distribution about an infinite cylinder. For rectangular wings the lift-curve slope is found to be

$$(C_{L_{\alpha W}})_b = \frac{4}{\beta} \left(\frac{n+1}{n} \right) \left(1 - \frac{1}{2A\beta} \right) \quad (3)$$

From figure 6, equation (1) is obviously inadequate in its assumption of 2α over the body and is presented only to show the upper limit of these simple approximations. Both equations (2) and (3) show good

agreement with experiment at the higher aspect ratios; however, only equation (2) shows the correct trends with decreasing aspect ratio. It can be seen that each of these approximations is inadequate at the lower aspect ratios. At low aspect ratios, three-dimensional effects are predominant with more complex flow interactions present such that it would not be expected that these approximations would give correct values of lift-curve slope. The experimental values at $\frac{L}{c} = 4.55$ show best agreement with theory because for this condition the body flow about the wing is probably more nearly that of the flow about an infinite cylinder.

Drag.- It should be pointed out that the drag data are subject to the most variation with Reynolds number; thus, only qualitative observations from these results are of significance. In this investigation the Reynolds number was 2.80×10^6 based on the body length and 0.19×10^6 based on the wing chord.

In an attempt to obtain some general effects of geometry on the drag results, several analyses were made. Values of incremental tail drag, both in and out of the presence of the wing, were obtained and plotted against actual tail angle, including in the tail angle the actual average downwash angle obtained from the tests, as discussed later. The results showed no consistent trends, but did show that the effect on the incremental tail drag of adding the wing was small. The drag coefficient at about 2° angle of attack decreased slightly as the wing was moved rearward as a result of the wing inducing transition with turbulent flow over the portion of the body rear of the wing. Moving the wing rearward would result in a smaller portion of the body having a turbulent boundary layer.

Downwash Results

Theoretical considerations.- It has been shown by several recent investigations (references 6 to 10) that the simplified concepts used in applying the linearized theory to the calculation of the flow field behind a lifting surface are not adequate except at small angles of attack and must be modified to account for the movement of the vortex sheet. These investigations show that both the displacement and the rolling-up of the vortex sheet must be taken into account in applying the linear theory. Since in this investigation the experimental downwash results were average values over the tail span, it was felt that the extensive calculations necessary to locate accurately the vortex sheet were not justified. Thus, only the simple displacement correction was made that the vortex sheet was contained in a streamwise plane passing through the wing trailing edge.

The theoretical calculation presented in reference 11 of the flow field behind a rectangular wing was used in the present calculations. From these results, plots of the variation of flow angle over the tail span at different vertical locations relative to the plane of the wing were obtained. Average downwash angles over the tail span at the different vertical locations were found and plots of $\frac{d\epsilon}{d\alpha}$ against α were made for each configuration. In the present calculations the downwash distribution at infinity was used. The use of this distribution gave average downwash angles slightly higher than would have been obtained had the downwash distribution at finite distances been used.

Experimental method of obtaining average downwash angles.— The experimental force data may be reduced to give average downwash angles at the tail by the following procedure: The lift of the BT configuration, where the tail lift is assumed to be changed only by a change in flow angle at the tail, is summed as follows:

$$C_{L_{BT}} = C_{L_B} + C_{L_T} = C_{L_B} + C_{L_{\alpha T}}(\alpha - \epsilon_b) \quad (4)$$

The change in tail lift with angle of flow at the tail, $C_{L_{\alpha T}}$, is measured as $\left(\frac{\partial C_L}{\partial i_t}\right)_b$. If $\left(\frac{\partial C_L}{\partial i_t}\right)_b$ is a function of α , at any angle of attack α_n the lift of the BT configuration may be written as

$$C_{L_{BT}} = C_{L_B} + \int_{\alpha=0}^{\alpha_n} \left(\frac{\partial C_L}{\partial i_t}\right)_b d(\alpha - \epsilon_b) \quad (5)$$

or

$$C_{L_{BT}}(\alpha_n) = C_{L_B}(\alpha_n) + \sum_{K=0}^n \left[\frac{\partial C_L}{\partial i_t} \left(\alpha_{K+\frac{1}{2}} \right) \right]_b \left[(\alpha_{K+1} - \alpha_K) - (\epsilon_{K+1} - \epsilon_K)_b \right] \quad (6)$$

where K is the number of steps in the numerical integration from $\alpha = 0$ to α_n .

A similar equation may be written for the lift of the BWT configuration as follows:

$$C_{L_{BWT}}(\alpha_n) = C_{L_{BW}}(\alpha_n) + \sum_{K=0}^n \left[\frac{\partial C_L}{\partial i_t} \left(\alpha_{K+\frac{1}{2}} \right) \right]_{bw} \left[(\alpha_{K+1} - \alpha_K) - (\epsilon_{K+1} - \epsilon_K)_{bw} \right] \quad (7)$$

These equations are solved for ϵ_b and ϵ_{bw} , and the downwash due to adding the wing is thus the difference between the two values; that is,

$$\epsilon_w = \epsilon_{bw} - \epsilon_b \quad (8)$$

The ϵ_w values obtained using these equations contain the effects on the average flow angle at the tail of velocity gradients in the region of the tail and mutual interference between the body-induced flow and the wing-induced flow at the tail.

Also included in the experimental ϵ_w values are the effects of assuming that the lift increment on the body due to the tail is the same for a change in incidence angle as for a change in angle of attack. For these configurations this lift increment is small; thus, even large differences between the lift increment on the body due to varying incidence angle and due to varying angle of attack will have only a secondary effect upon the experimental average downwash results.

Experimental downwash results.- The results of calculations made using the above procedure are shown in figure 7 and the ϵ_w values are compared with approximate theoretical values for the isolated wing-tail case. The average upwash due to the body ϵ_b is given for the long-span tail in figure 7(a) and for the short-span tail in figure 7(i). The upwash for both tail spans is nearly linear with a small decrease at the highest angles of attack. The larger upwash shown for the short-span tail is as might be expected from the distribution of upwash about the body. Since for these tail locations the upwash can be assumed to be equal to R^2/r^2 , where r is the distance out from the body and R is the radius of the body, the shorter-span tail would leave the largest value of average upwash.

For the largest-aspect-ratio wing, model 1, the average wing downwash is seen to be small for both tail lengths. The experimental downwash angles show a greater change with angle of attack than do the theoretical values with negative values of $\partial\epsilon/\partial\alpha$ shown at the higher angles of attack.

Decreasing the aspect ratio, model 2, results in somewhat higher values of ϵ_w . The experimental average downwash angles show a decrease in $\partial\epsilon/\partial\alpha$ near zero with decreasing tail arm which is not indicated by the theoretical values at infinity. However, reference 11 shows that in the plane of the wing similar trends occur with decreasing tail length. The flattening of the ϵ_w curves at the higher angles of attack results from the slope of the vortex sheet being nearly constant

with angle of attack (reference 12). Thus, although $\partial \epsilon / \partial \alpha$ would be nearly zero, ϵ_w may have finite values, as is shown for this configuration.

For model 3, where the wing span is equal to the tail span, the average downwash is increased somewhat. As in the results of model 2, decreasing downwash with decreasing tail arm is shown but the change is much smaller. The results of reference 11 show that, as the wing aspect ratio is reduced, the change with tail arm becomes smaller. It is probable that the effects of the rolling-up of the vortex sheet have begun to appear in this case. The rolling-up of the vortex sheet would move the points of concentrated vorticity and upwash regions inboard of the tail tip and alleviate the downward displacement of the vortex sheet as a whole (see references 10, 12, and 13). The upwash regions and points of concentrated vorticity also tend to move farther inboard with increasing angle of attack as has been shown in reference 12. These effects may be evidenced by the trend of the ϵ_w curves toward zero as α increases. Negative values of $\partial \epsilon / \partial \alpha$ are shown at the higher angles of attack.

Decreasing the wing span to less than the tail span, model 4, results in a decrease in average downwash for the long-tail-arm case and little change for the short tail arm. The decreased average downwash for the long tail arm is due to the increased upwash over the tail tip sections. Since the vortex cores tend to sweep inboard with increasing distance downstream of the wing, the short-tail-arm case would give larger average downwash angles. It is also probable that, as the wing aspect ratio is decreased from model 3 to model 4, the effects of increased upwash over the tip sections are compensated by the effects of larger displacement of the trailing vortex sheet. The larger displacement of the trailing vortex sheet would result in larger average downwash values for the short-tail-arm case since for this case the tail is closest to the trailing vortex sheet.

The wing span is again equal to the tail span in model 5 which results in a considerable increase in average downwash as compared with model 3 because of the smaller wing aspect ratio of model 5. Little difference between the two tail arms is shown except that the short-tail-arm case indicates slightly higher downwash values at the high angles of attack. This trend is similar to that shown for model 4 although the differences for model 4 are much greater.

For all configurations, the agreement between the experimental average downwash angles and the simple displacement correction applied to the linear theory is good at small angles of attack. At higher angles of attack, it is evident that a more adequate accounting for the movement of the vortex sheet is necessary.

Experimental tail effectiveness.- The variation in η_t with angle of attack is shown in figure 8. For models 1 to 4 this parameter is about 1 with fairly small effects of wing position indicated. Model 5, however, shows an increase in η_t to about 1.1 in the angle range above 8° . There is little difference in the effect shown for the two wing locations.

Pitching-Moment Results

The pitching-moment coefficients are referenced to a center-of-gravity location chosen to give equal values of $\partial C_m / \partial C_L$ at low angles of attack for all BWT configurations. For each BWT configuration at an angle of attack of about 2° , the center-of-gravity location was fixed at one body diameter ahead of the aerodynamic center.

The aerodynamic-center locations for the BWT and BW configurations are shown in figure 9. These locations are at an angle of attack of 2° and are given in chord lengths from the wing leading edge. A forward movement of the aerodynamic-center location with increasing aspect ratio is shown for the BWT configurations which is smallest for the short-tail-arm case. In this case the center of pressure of the incremental wing lift is closest to the center of pressure of the configuration. Decreasing the aspect ratio of the tail, model 5, moves the aerodynamic center forward as is shown by the flagged symbols.

The effect of wing on the tail as shown in the pitching moment of the BWT configurations is illustrated in figure 10. The dashed curves are given as a base or "no-effect-of-wing-on-tail reference." These curves are obtained by adding the incremental tail moments in the presence of the body ($C_{m_{BT}} - C_{m_B}$) to the measured pitching moment for the BW configuration. Thus, the difference between the dashed curves and the curves for the measured pitching moment of the complete BWT configuration shows the effect of adding the wing. The experimental and calculated pitching-moment curves have been shifted to the case of $i_t = 0^\circ$ for ease of comparison.

The effect of wing downwash upon the pitching-moment contribution of the tail may be considered as follows: If the change in pitching-moment contribution of the tail in the presence of the wing with flow angle at the tail is measured as $\left(\frac{\partial C_m}{\partial i_t}\right)_{bw}$, then the effect of wing downwash on the pitching moment is given as $\left(\frac{\partial C_m}{\partial i_t}\right)_{bw} \epsilon_w$. Values of $\frac{\partial C_m}{\partial i_t}$ were used in this analysis instead of values of $\frac{\partial C_L}{\partial i_t}$ because the selection of an arbitrary tail center-of-pressure-location was avoided. Experimental

values of ϵ_w were used and the results are given as symbols in figure 10.

For all configurations, good agreement is shown between the measured pitching moment and calculated pitching moment particularly in the low angle-of-attack range. Thus, as might be expected, the effect of the wing on the tail is seen to be primarily downwash, that is, a change in the average flow angle at the tail. Some effects of changes in η_t are shown at the higher angles of attack with a sizeable effect shown for model 5. At angles of attack over 8° a sizeable stabilizing moment is shown for both wing positions of model 5 which is the result of the increase in η_t to approximately 1.1.

CONCLUSIONS

Tests at a Mach number of 1.93 of several missile configurations having rectangular wings and tails of various spans have indicated the following results:

1. At small angles of attack, average downwash angles at the tail, obtained from experimental lift results, agreed well with the linear theory for an isolated wing-tail arrangement when a simple correction for displacement of the vortex sheet was included. At higher angles, however, large differences between theory and experiment indicated that a better method of accounting for the displacement and distortion of the trailing vortex sheet and for the effects of the body was necessary. For most configurations, the experimental curves of downwash due to addition of the wing ϵ_w against angle of attack α reached a maximum in the range of angle of attack from 4° to 7° and then decreased, thus giving negative values of $\partial\epsilon_w/\partial\alpha$.

2. Comparison of the experimental lift-curve slope of the wing in the presence of the body with several approximate theoretical estimates showed the theories to be inadequate at low aspect ratios, probably because of the complexity of the associated three-dimensional flows. Agreement at the higher aspect ratios was good for those estimates assuming that the body carried the same lift over the included part of the wing as would be developed by the wing without the body.

3. The effect of the addition of the wing upon the pitching-moment contribution of the tail was principally one of downwash; that is, a change in the average flow angle at the tail.

Langley Aeronautical Laboratory
National Advisory Committee for Aeronautics
Langley Air Force Base, Va.

REFERENCES

1. Ellis, Macon C., Jr., and Grigsby, Carl E.: Aerodynamic Investigation at Mach Number 1.92 of a Rectangular Wing and Tail and Body Configuration and Its Components. NACA RM L9L28a, 1950.
2. Nash, E. M., and Williams, R. H.: First Supersonic Wind Tunnel Tests on a Model of the MX-904 Missile. Rep. No. 40-104-A, Hughes Aircraft Co., Nov. 1948.
3. Speth, Robert F.: Results of Rascal Supersonic Wind Tunnel Tests at $M = 1.72$. Rep. No. 56-980-001, Bell Aircraft Corp., Dec. 20, 1948.
4. Speth, Robert F.: Results of Rascal Supersonic Wind Tunnel Tests at $M = 1.28$. Rep. No. 56-980-001, Bell Aircraft Corp., Dec. 20, 1948.
5. Stewart, Homer J., and Meghreblian, Robert V.: Body-Wing Interference in Supersonic Flow. Progress Rep. No. 4-99, Jet. Propulsion Lab., C.I.T., June 2, 1949.
6. Perkins, Edward W., and Canning, Thomas N.: Investigation of Downwash and Wake Characteristics at a Mach Number of 1.53.
I - Rectangular Wing. NACA RM A8L16, 1949.
7. Perkins, Edward W., and Canning, Thomas N.: Investigation of Downwash and Wake Characteristics at a Mach Number of 1.53.
II - Triangular Wing. NACA RM A9D20, 1949.
8. Perkins, Edward W., and Canning, Thomas N.: Investigation of Downwash and Wake Characteristics at a Mach Number of 1.53.
III - Swept Wings. NACA RM A9K02, 1950.
9. Cummings, J. L., Mirels, H., and Baughman, L. E.: Downwash in Vortex Region behind Trapezoidal-Wing Tip at Mach Number 1.91. NACA RM E9H15, 1949.
10. Adamson, D., and Boatright, William B.: Investigation of Downwash, Sidewash, and Mach Number Distribution behind a Rectangular Wing at a Mach Number of 2.41. NACA RM L50G12, 1950.
11. Lagerstrom, P. A., Graham, Martha E., and Grosslight, G.: Downwash and Sidewash Induced by Three-Dimensional Lifting Wings in Supersonic Flow. Rep. No. SM-13007, Douglas Aircraft Co., Inc., April 14, 1947.

12. Spreiter, John R., and Sacks, Alvin H.: The Rolling Up of the Trailing Vortex Sheet and Its Effect on the Downwash behind Wings. Preprint no. 250, Inst. Aero. Sci., Inc., Jan. 1950.
13. Mirels, Harold, and Haefeli, Rudolph C.: Line-Vortex Theory for Calculation of Supersonic Downwash. NACA TN 1925, 1949.

TABLE I.- PERTINENT MODEL DIMENSIONS

Configuration	Wing				Tail				Wing location, l/c	Center-of-gravity location, x/c
	Span, b (in.)	Chord, c (in.)	Area, S (sq in.)	Aspect ratio, A	Span, b_t (in.)	Chord, c_t (in.)	Area, S_t (sq in.)	Aspect ratio, A_t		
Model 1	4.067	0.590	2.400	6.89	2.507	0.622	1.558	4.03	7.08	7.53
									4.55	5.94
Model 2	3.325	.590	1.962	5.64	2.507	.622	1.558	4.03	7.08	7.45
									4.55	5.91
Model 3	2.574	.590	1.519	4.36	2.507	.622	1.558	4.03	7.08	7.19
									4.55	5.87
Model 4	1.831	.590	1.081	3.10	2.507	.622	1.558	4.03	7.08	6.93
									4.55	5.83
Model 5	1.831	.590	1.081	3.10	1.834	.622	1.141	2.95	7.08	7.82
									4.55	6.62

Fuselage ordinates:

$$\text{Station 0 to 3.125, } r = 1.40 \left[\frac{x}{6.25} - \left(\frac{x}{6.25} \right)^2 \right]$$

Station 3.125 to 6.625, constant diameter of 0.700

$$\text{Station 6.625 to 8.750, } r = 0.40 \left[\frac{8.75 - x}{4.25} - \left(\frac{8.75 - x}{4.25} \right)^2 \right] + 0.25$$

NACA

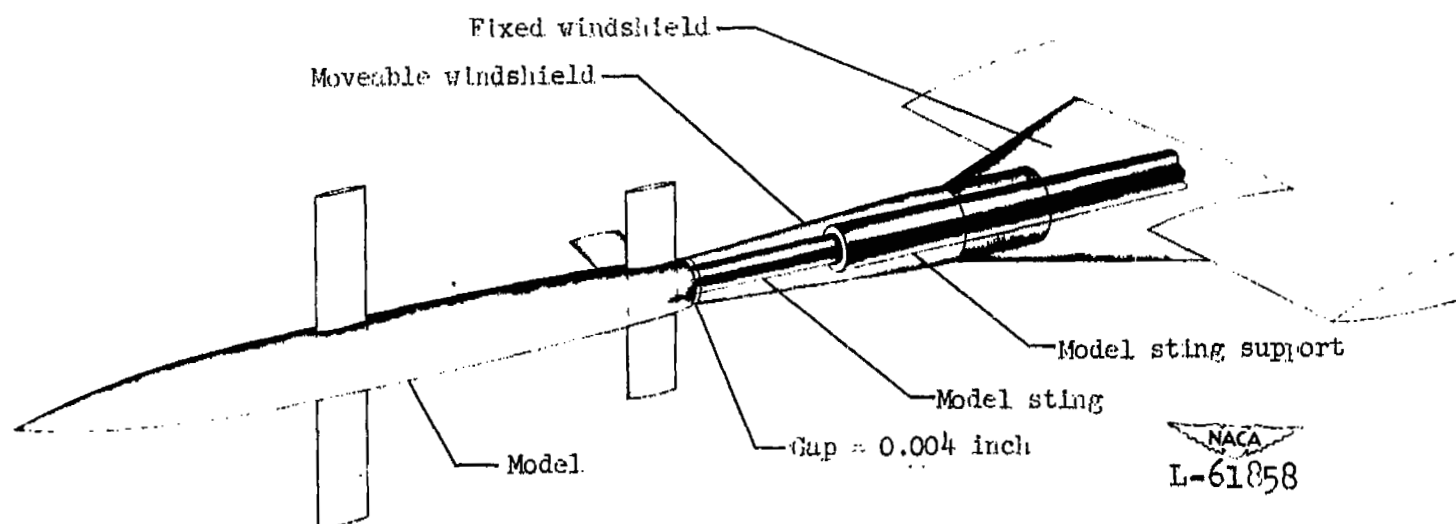


Figure 1.- Drawing of model support system.

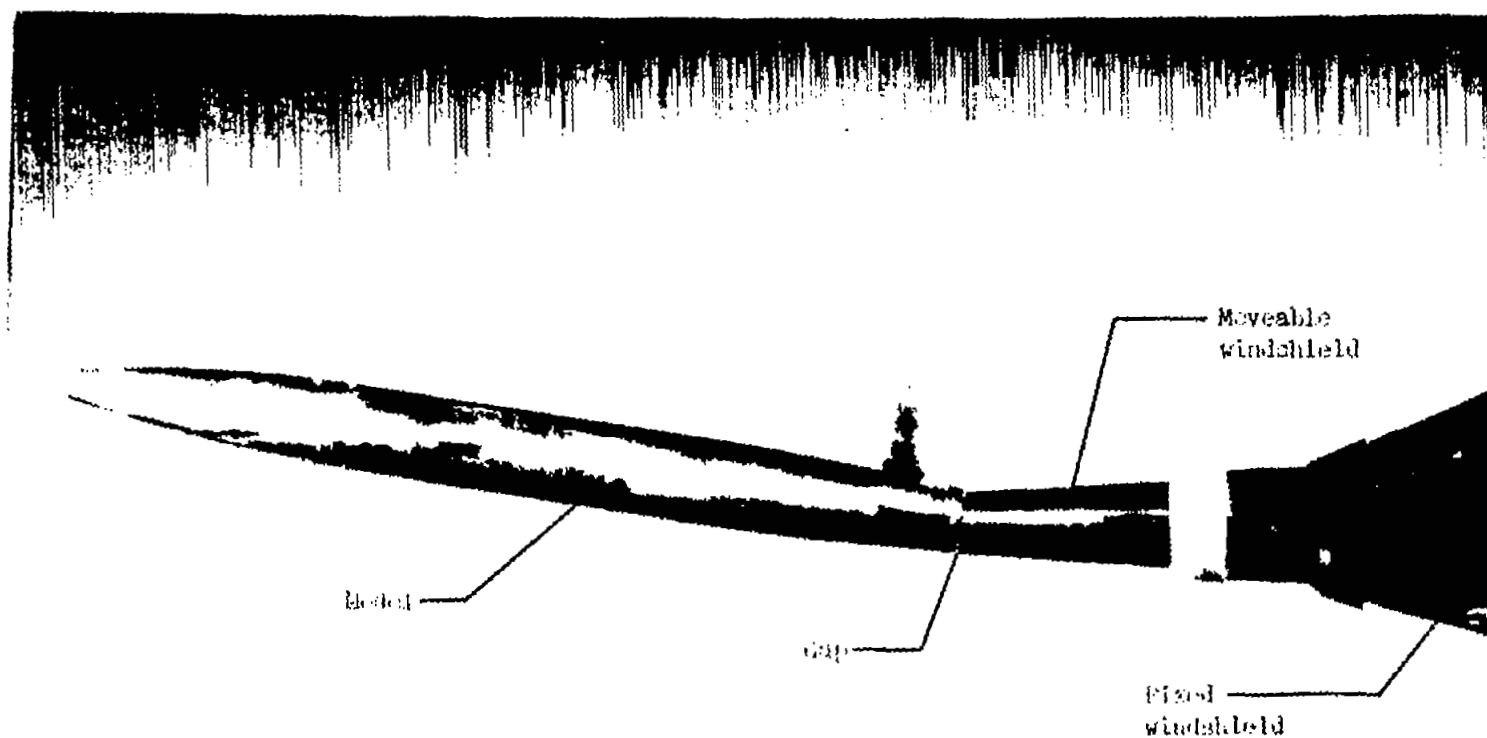
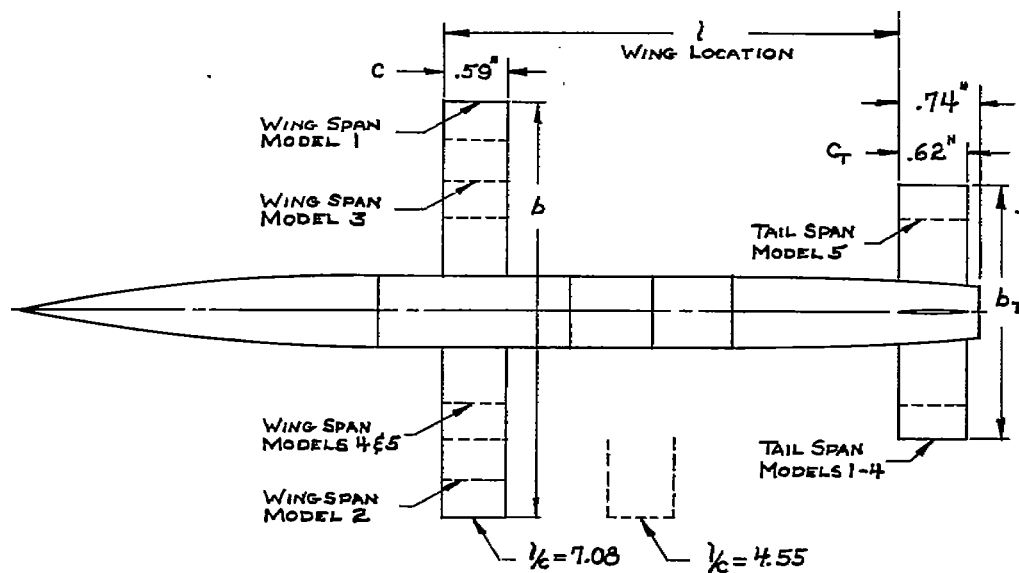
NACA
L-61933

Figure 2.- Top view of tunnel installation. Note: Gap is enlarged to show detail. For tests, Gap = 0.004 inch.



ALL LIFTING SURFACES
HAVE CIRCULAR-ARC
SECTIONS, $t/c = 6\%$.

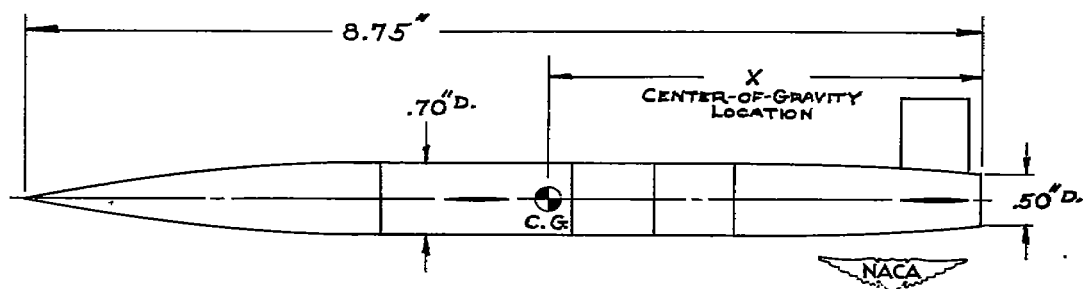
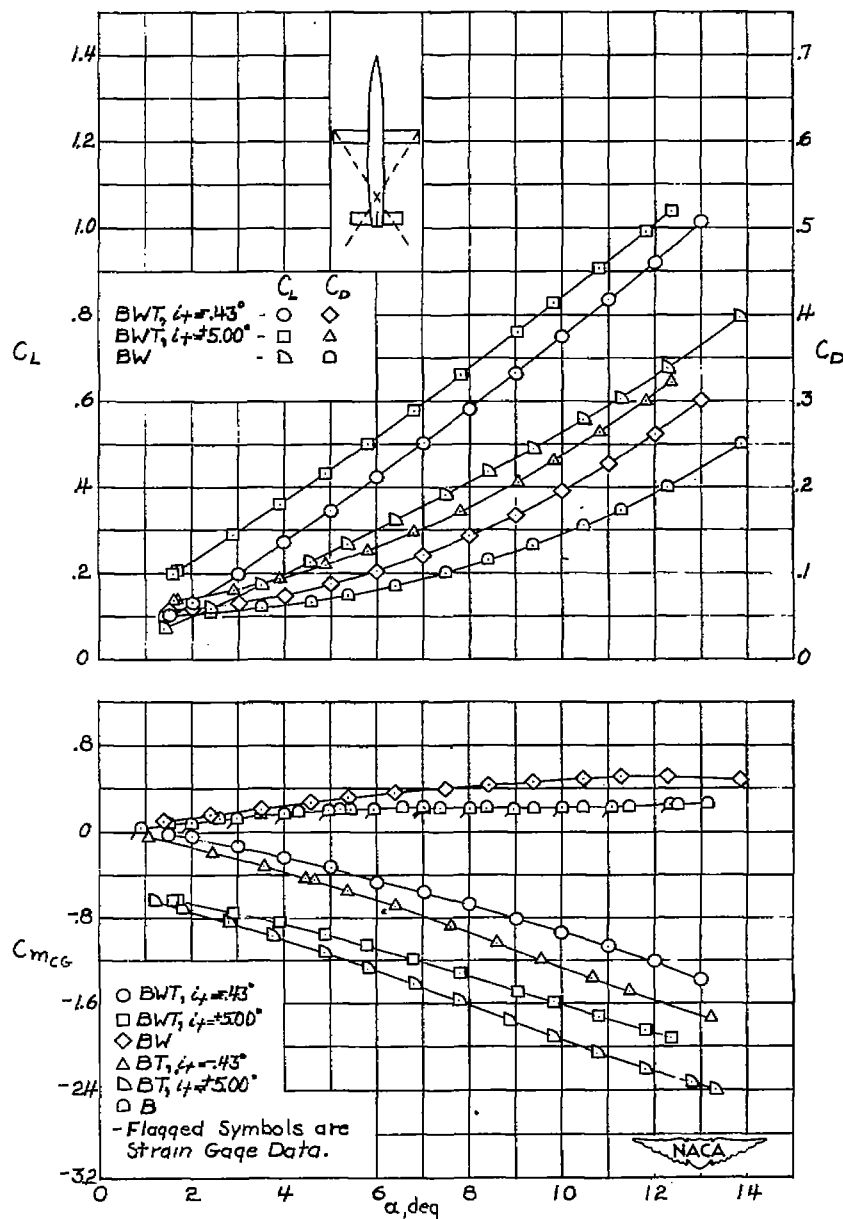
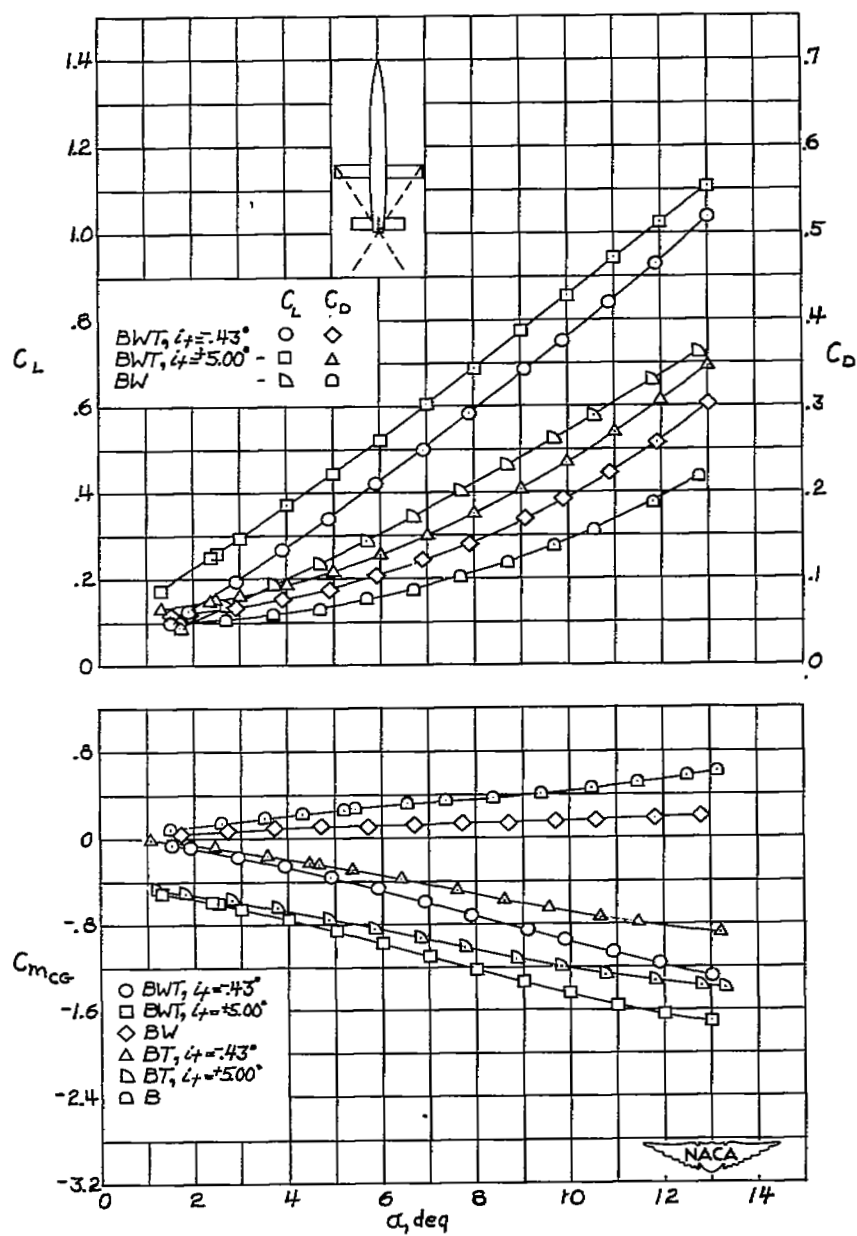


Figure 3.- Model drawing.



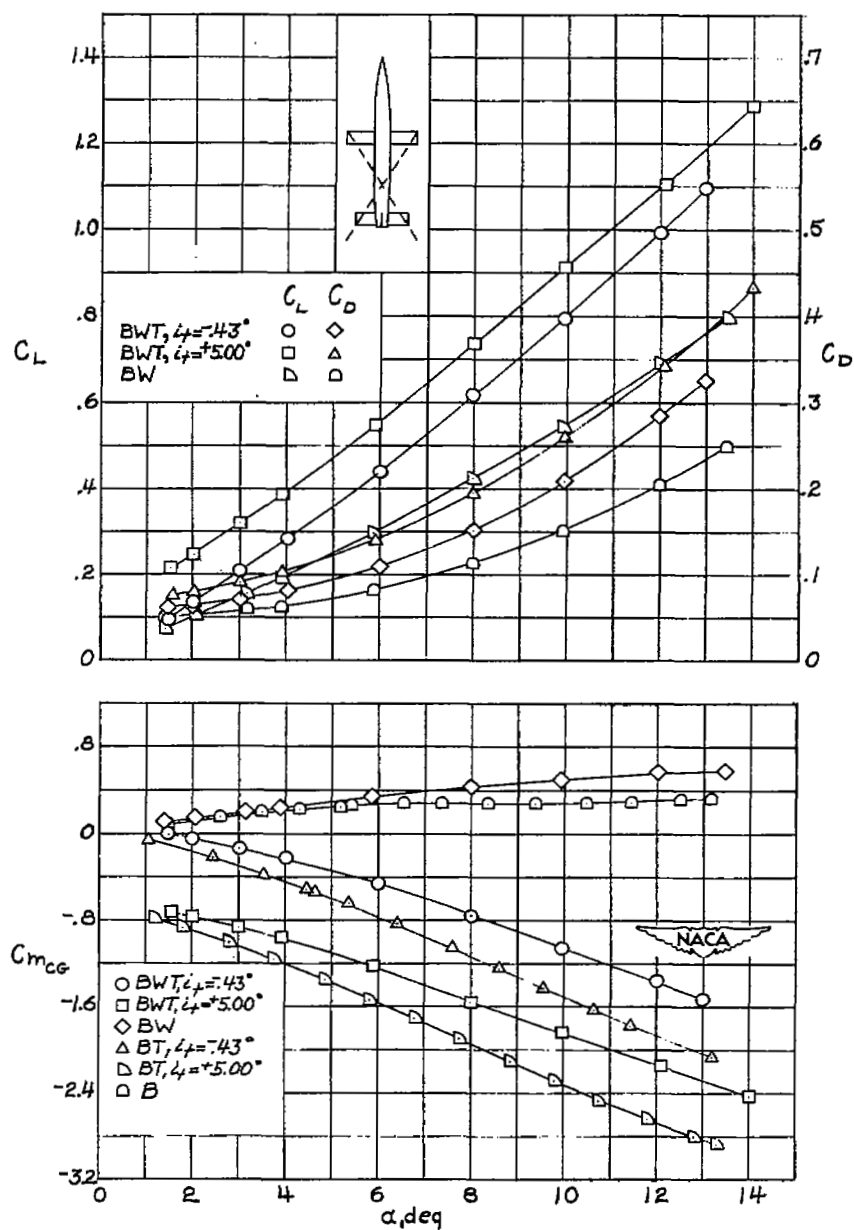
(a) Model 1, $\frac{l}{c} = 7.08$.

Figure 4.- Aerodynamic characteristics of BWT and BW configurations.
(Pitching-moment coefficient for BT and B included for comparison.)



(b) Model 1, $\frac{l}{c} = 4.55$.

Figure 4.- Continued.



(c) Model 2, $\frac{l}{c} = 7.08$.

Figure 4.- Continued.

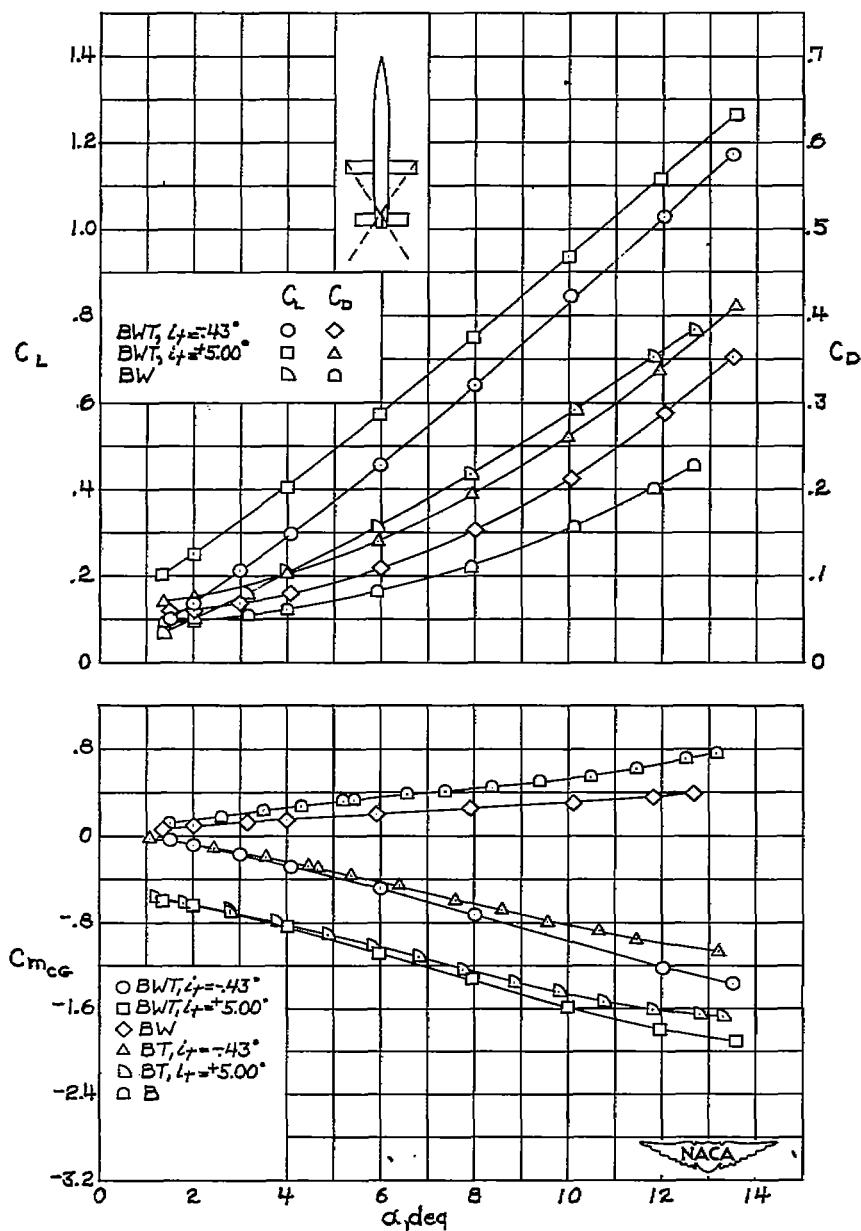
(d) Model 2, $\frac{l}{c} = 4.55$.

Figure 4.- Continued.

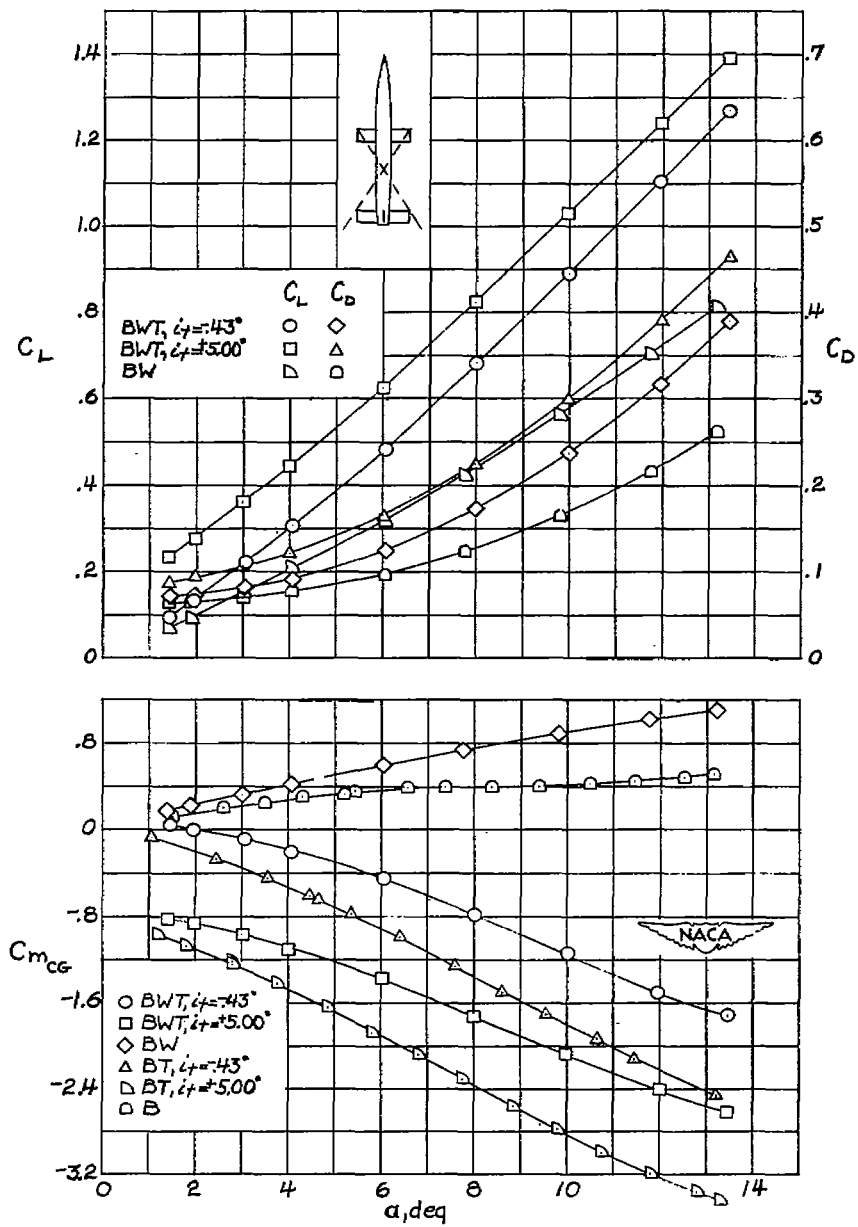
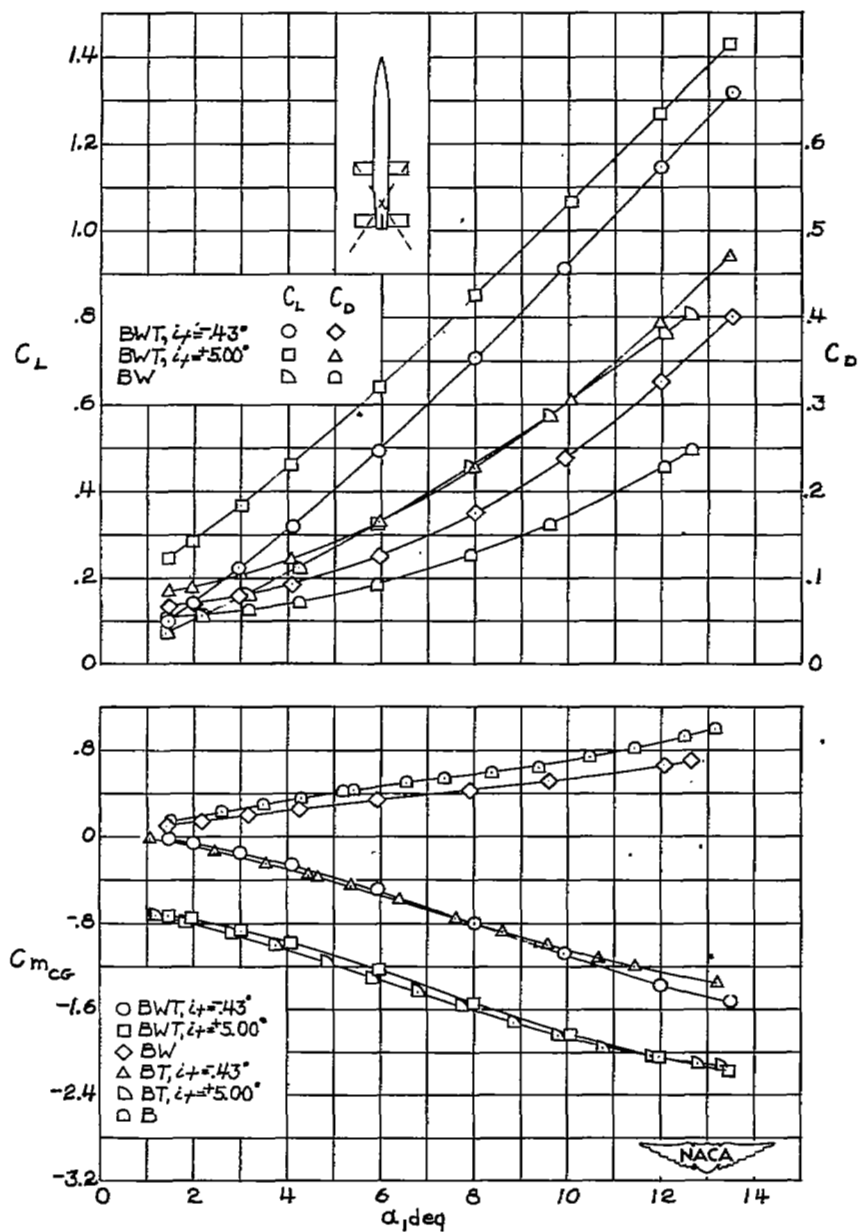
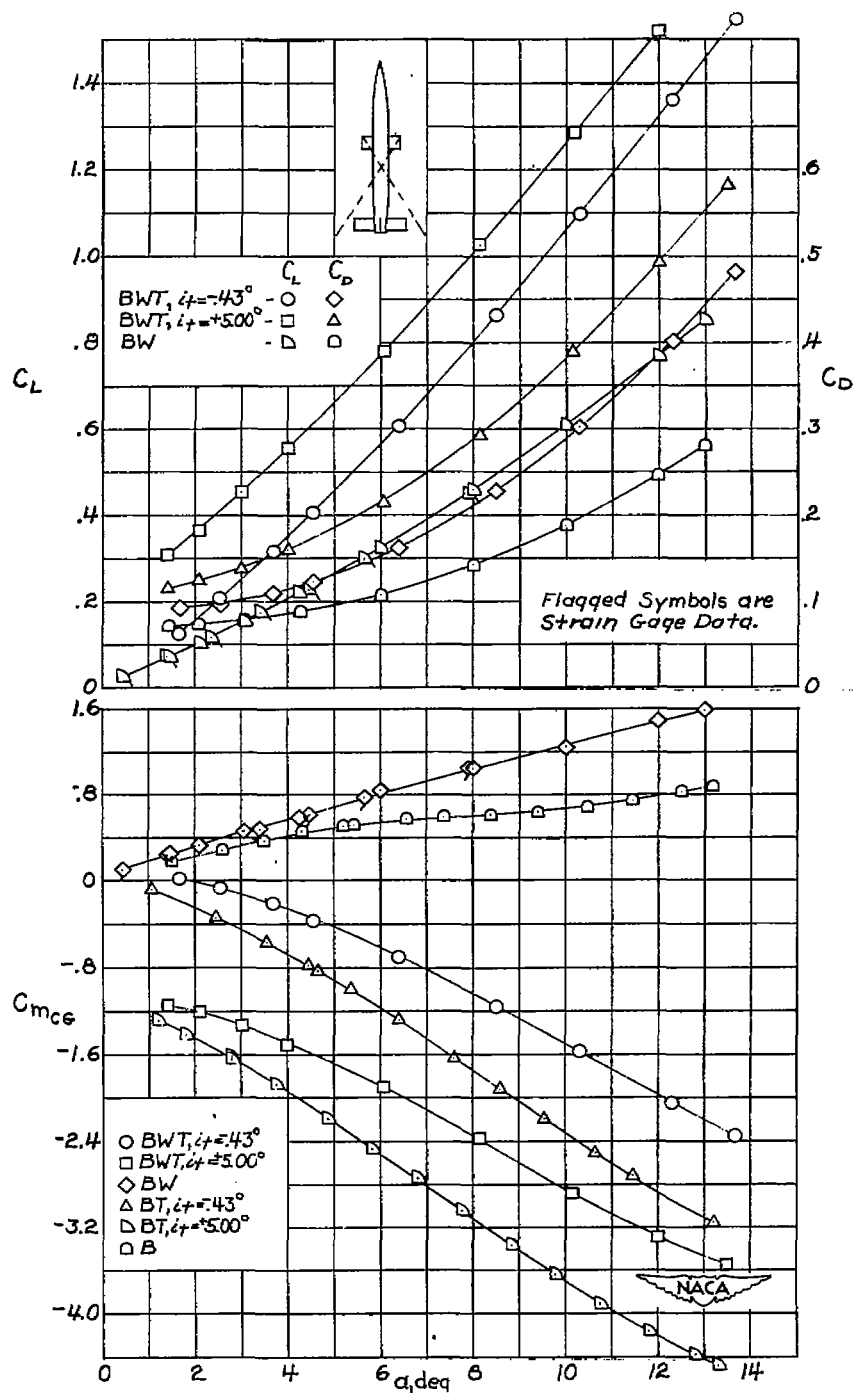
(e) Model 3, $\frac{l}{c} = 7.08$.

Figure 4.- Continued.



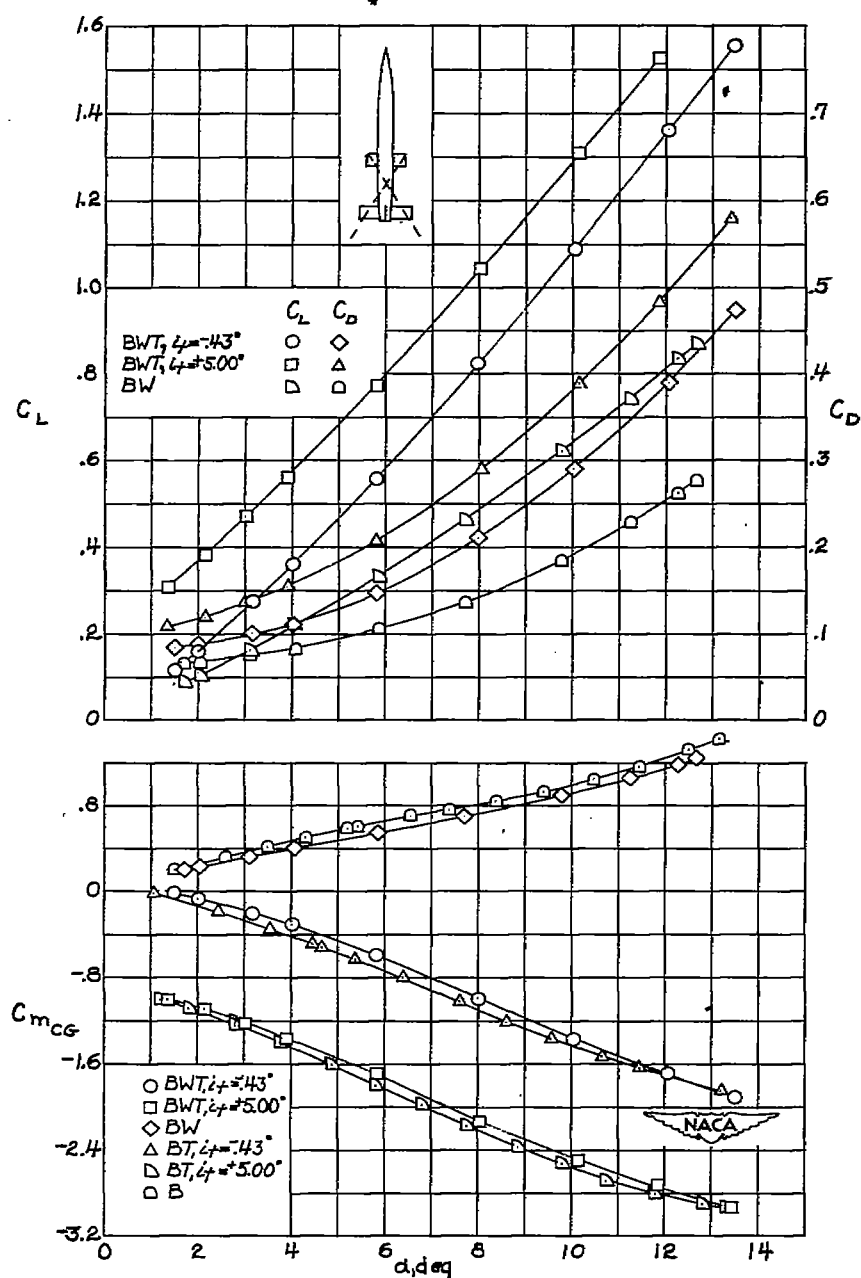
(f) Model 3, $\frac{l}{c} = 4.55$.

Figure 4.- Continued.



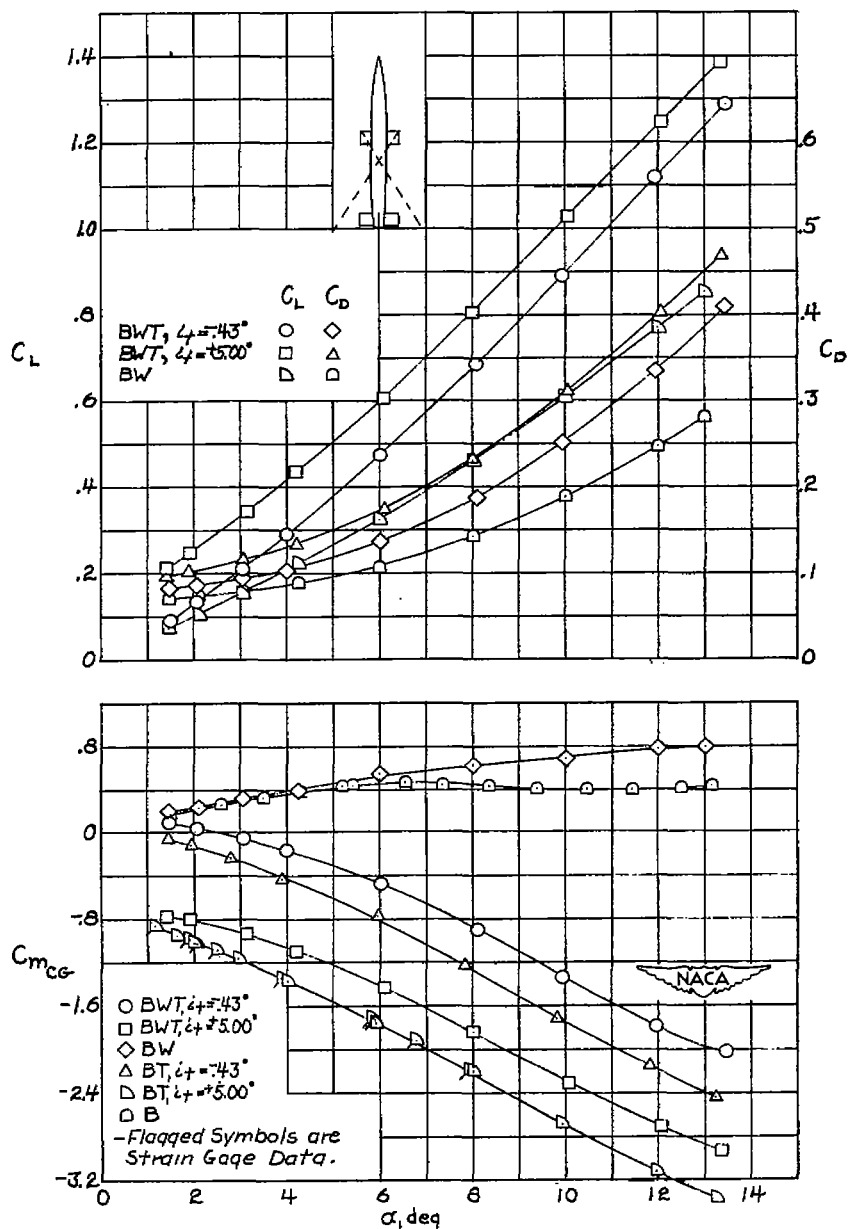
(g) Model 4, $\frac{l}{c} = 7.08$.

Figure 4.- Continued.



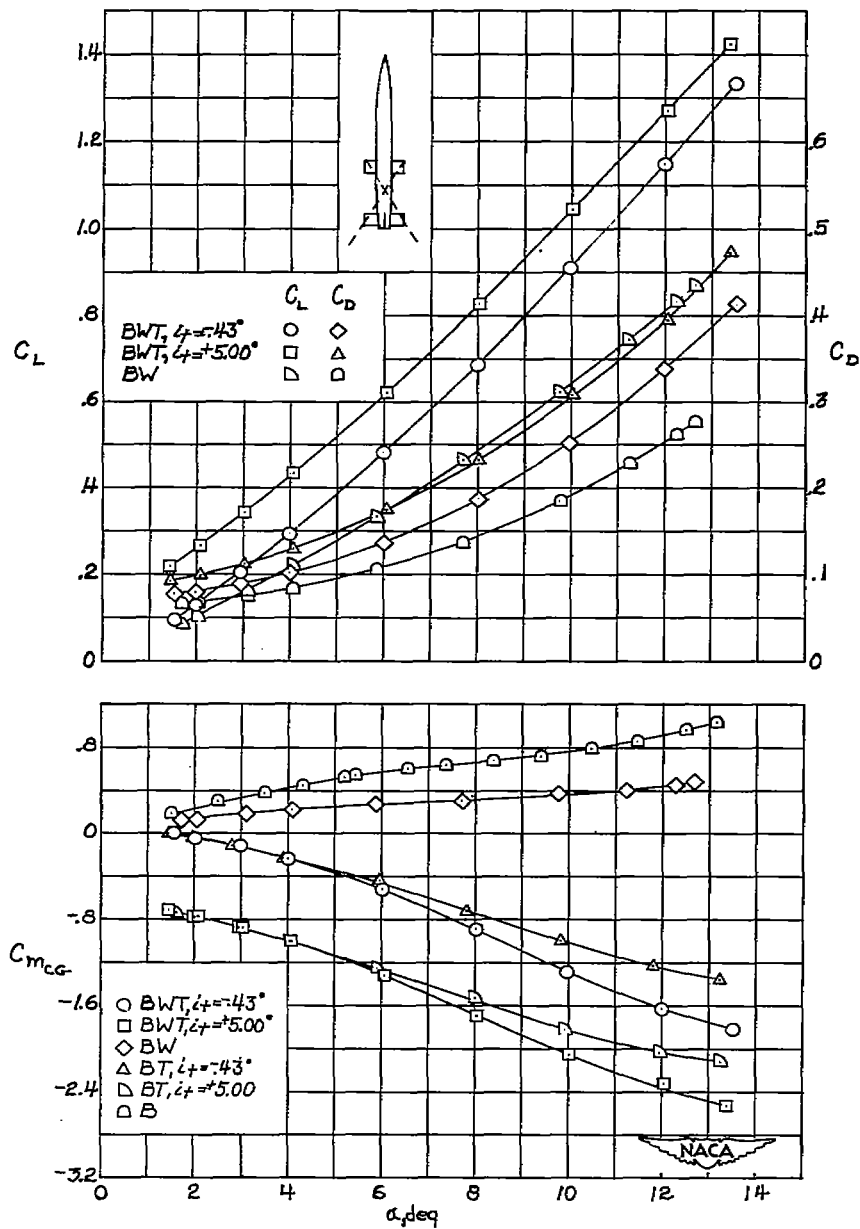
(h) Model 4, $\frac{l}{c} = 4.55$.

Figure 4.- Continued.



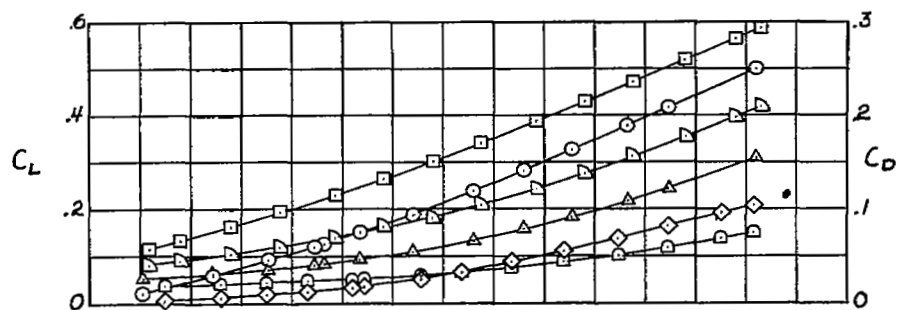
(1) Model 5, $\frac{l}{c} = 7.08$.

Figure 4.- Continued.

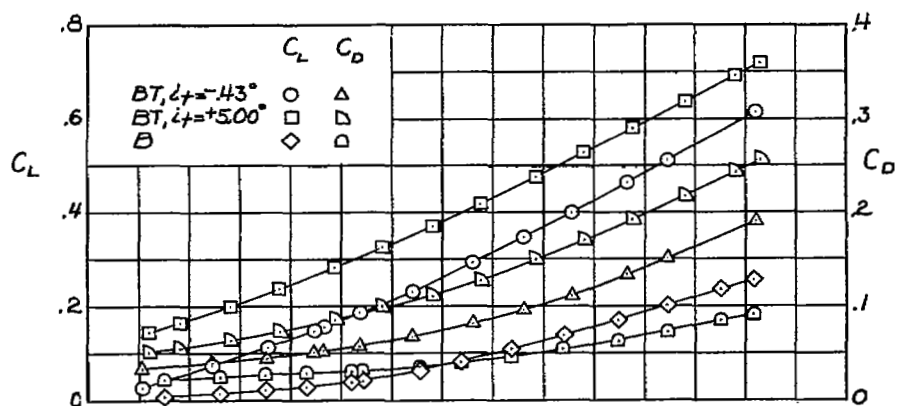


(j) Model 5, $\frac{l}{c} = 4.55$.

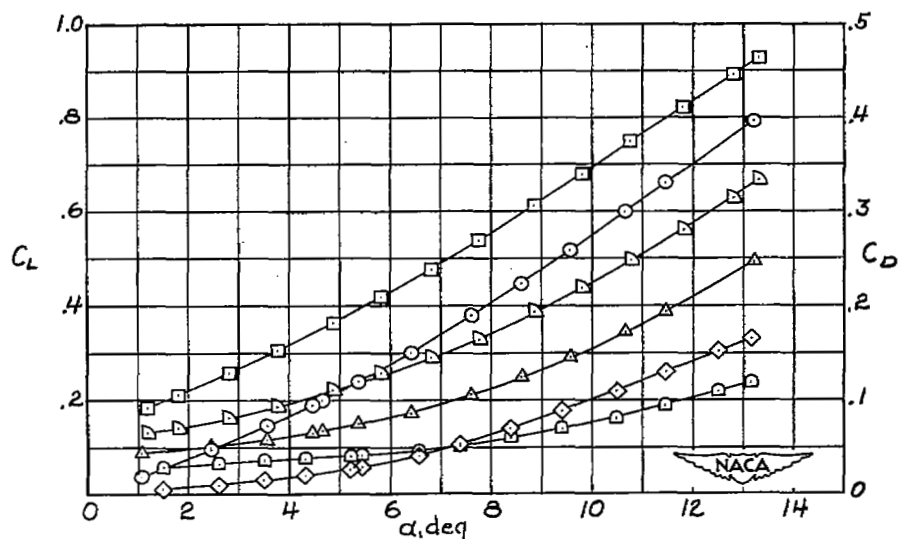
Figure 4.- Concluded.



(a) Model 1.

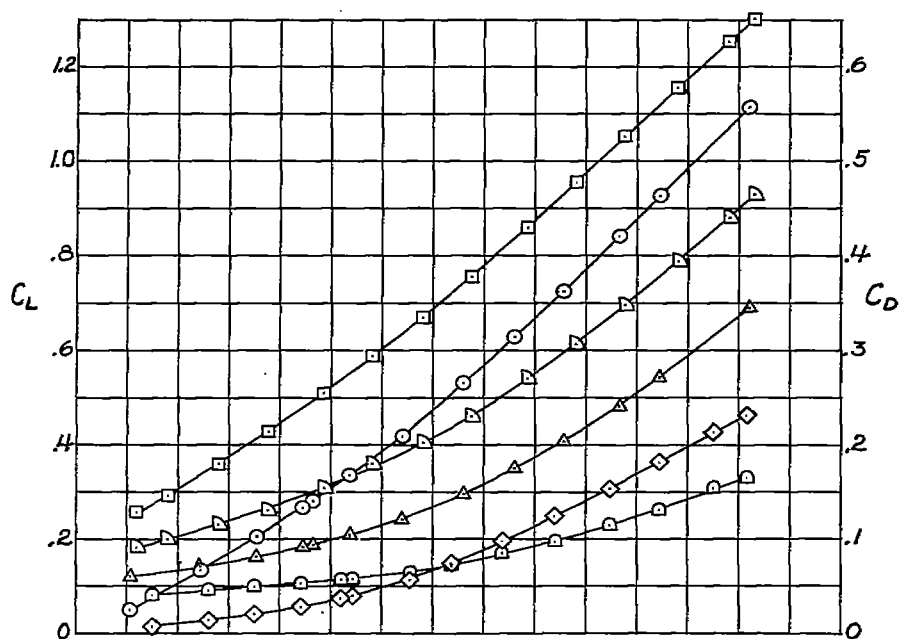


(b) Model 2.

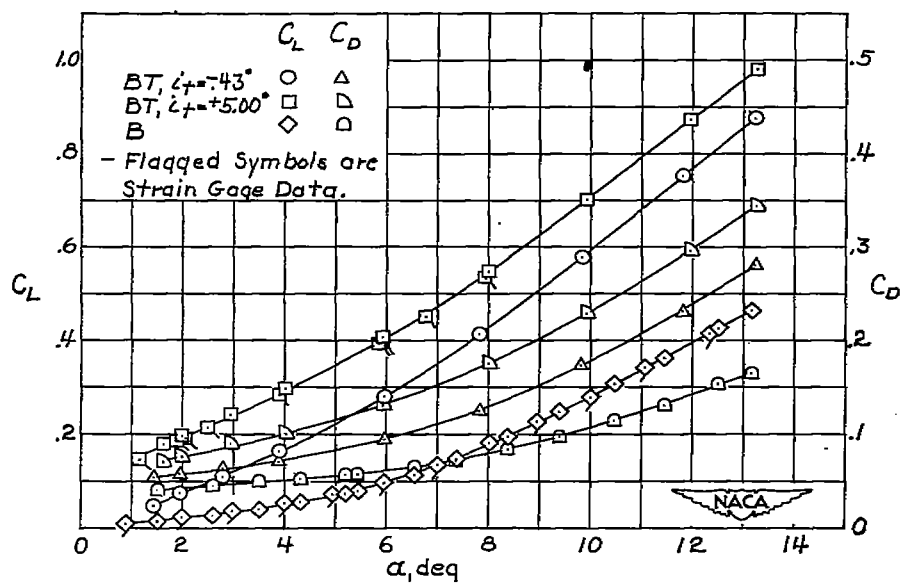


(c) Model 3.

Figure 5.- Variation of lift and drag coefficient with angle of attack for BT and B configurations.



(d) Model 4.



(e) Model 5.

Figure 5.- Concluded.

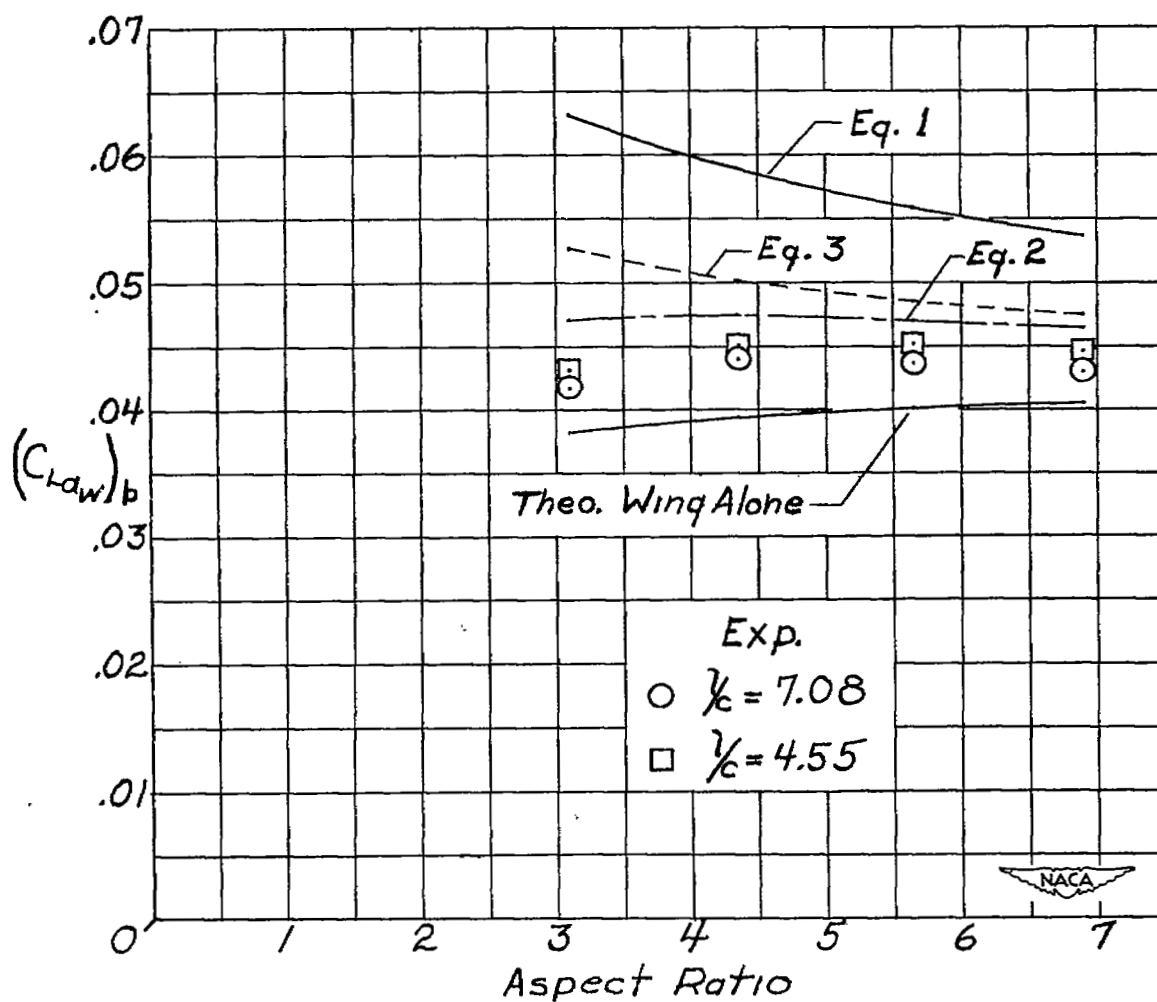


Figure 6.- Effect of body upwash on incremental lift-curve slope of rectangular wings.

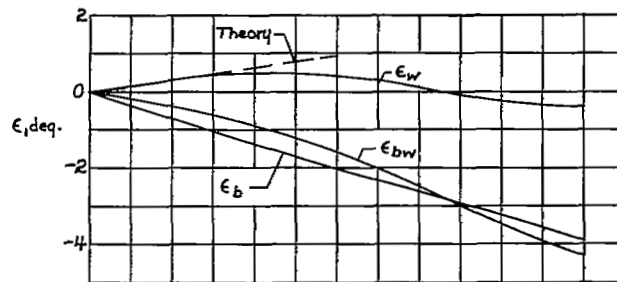
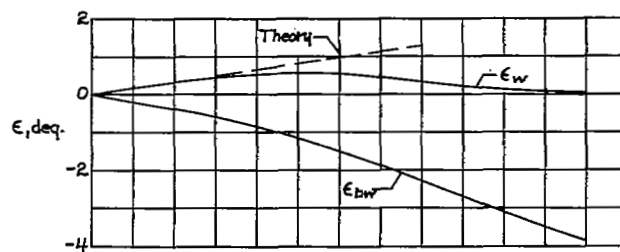
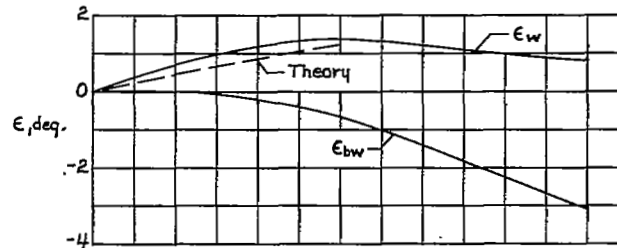
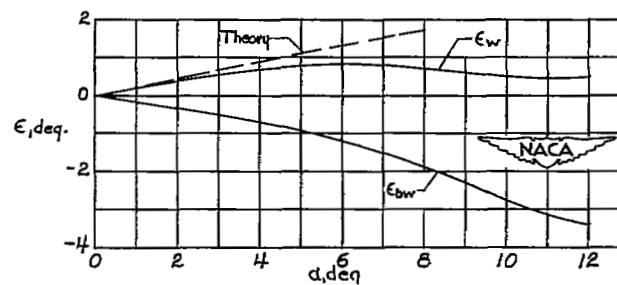
(a) Model 1, $\frac{l}{c} = 7.08$.(b) Model 1, $\frac{l}{c} = 4.55$.(c) Model 2, $\frac{l}{c} = 7.08$.(d) Model 2, $\frac{l}{c} = 4.55$.

Figure 7.- Variation of average downwash angles with angle of attack.

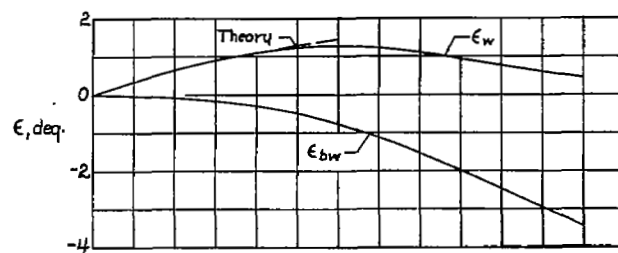
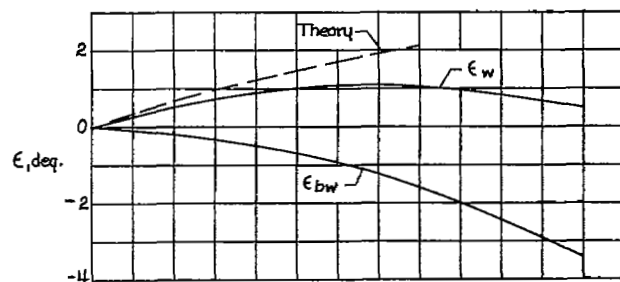
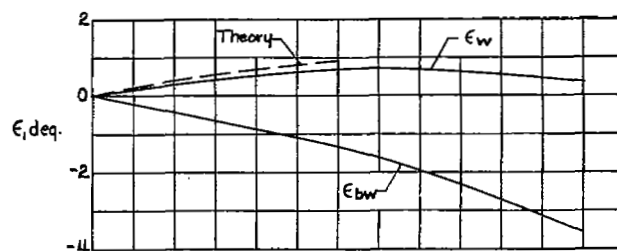
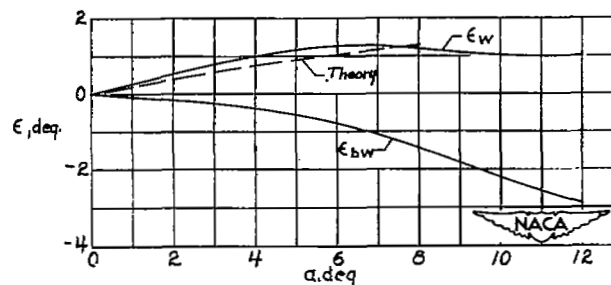
(e) Model 3, $\frac{l}{c} = 7.08$.(f) Model 3, $\frac{l}{c} = 4.55$.(g) Model 4, $\frac{l}{c} = 7.08$.(h) Model 4, $\frac{l}{c} = 4.55$.

Figure 7.- Continued.

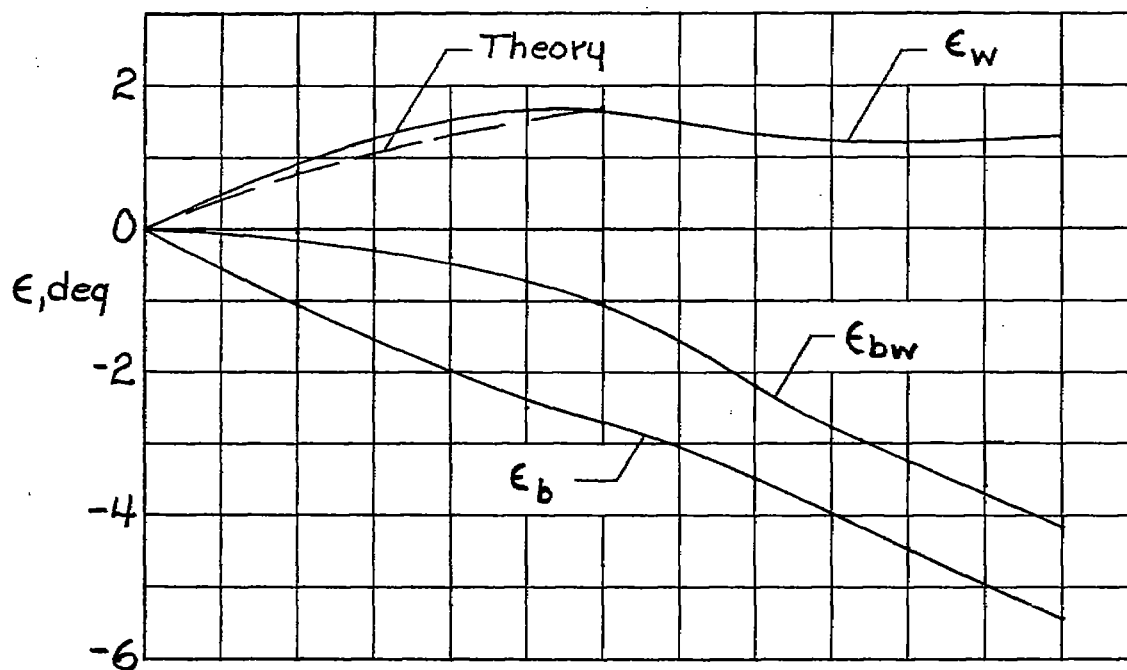
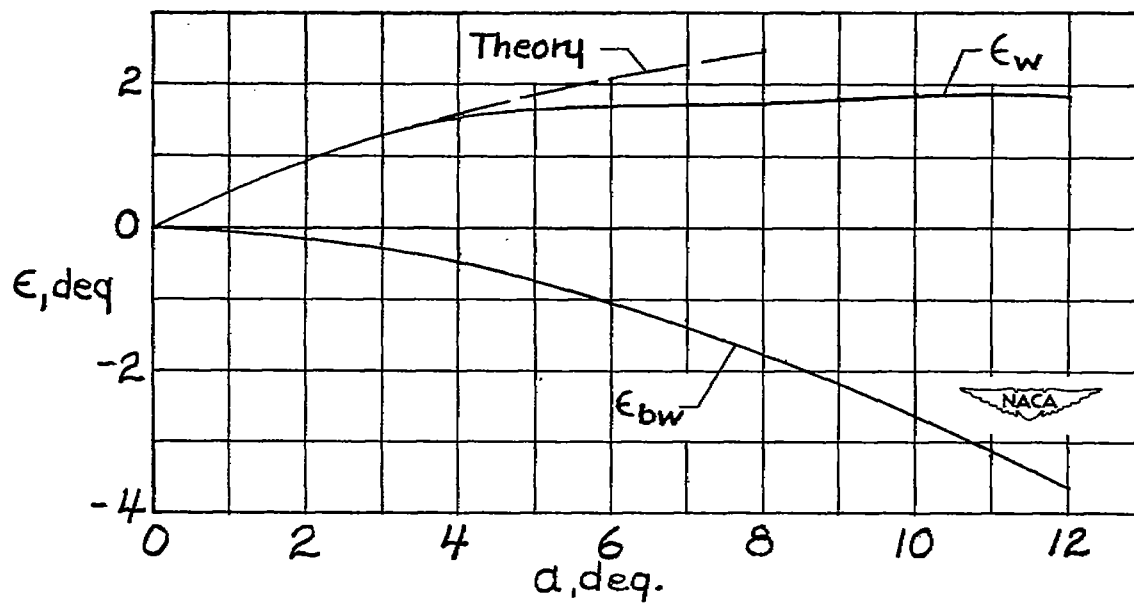
(i) Model 5, $\frac{l}{c} = 7.08$.(j) Model 5, $\frac{l}{c} = 4.55$.

Figure 7.- Concluded.

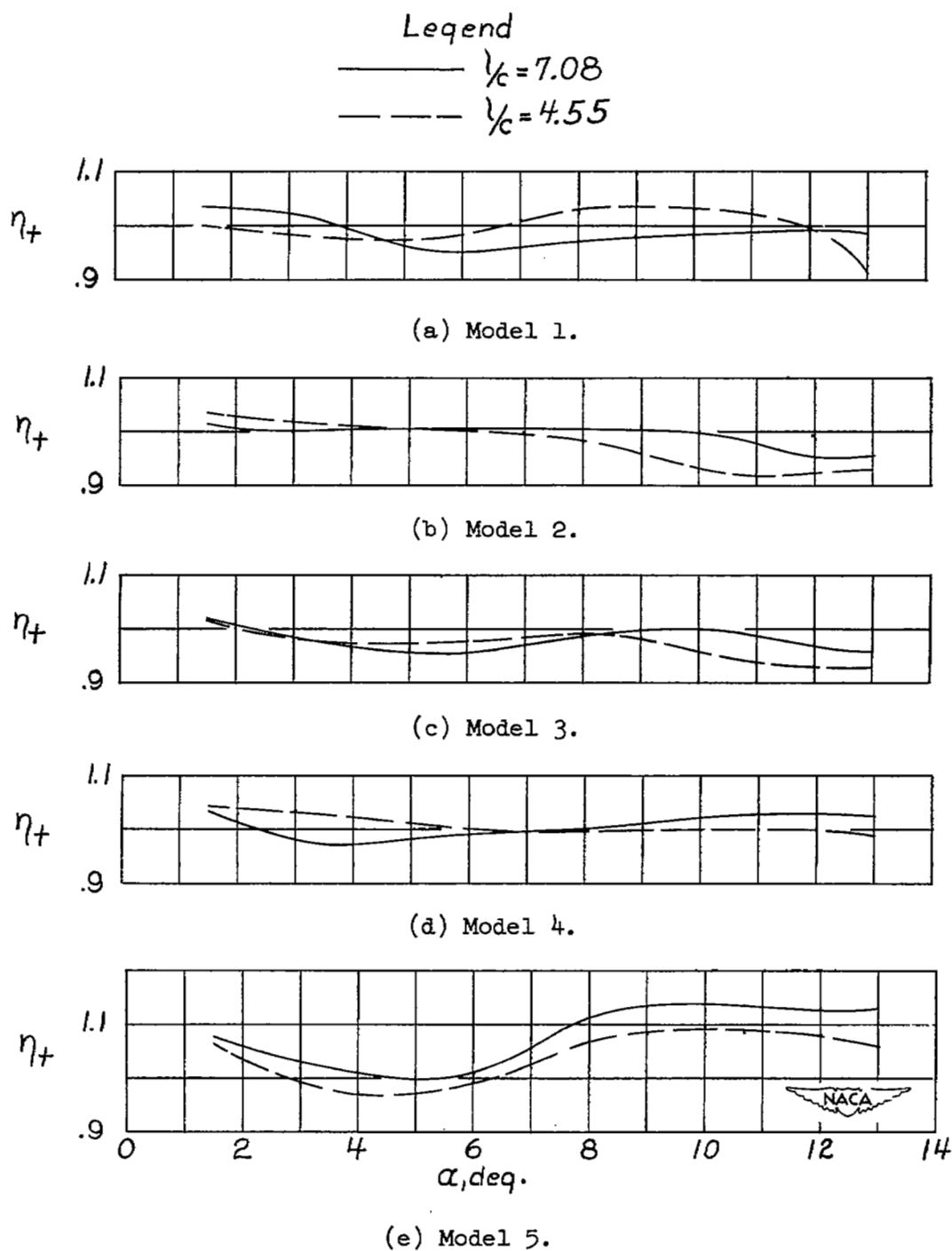


Figure 8.- Variation of wing wake parameter η_t with angle of attack.

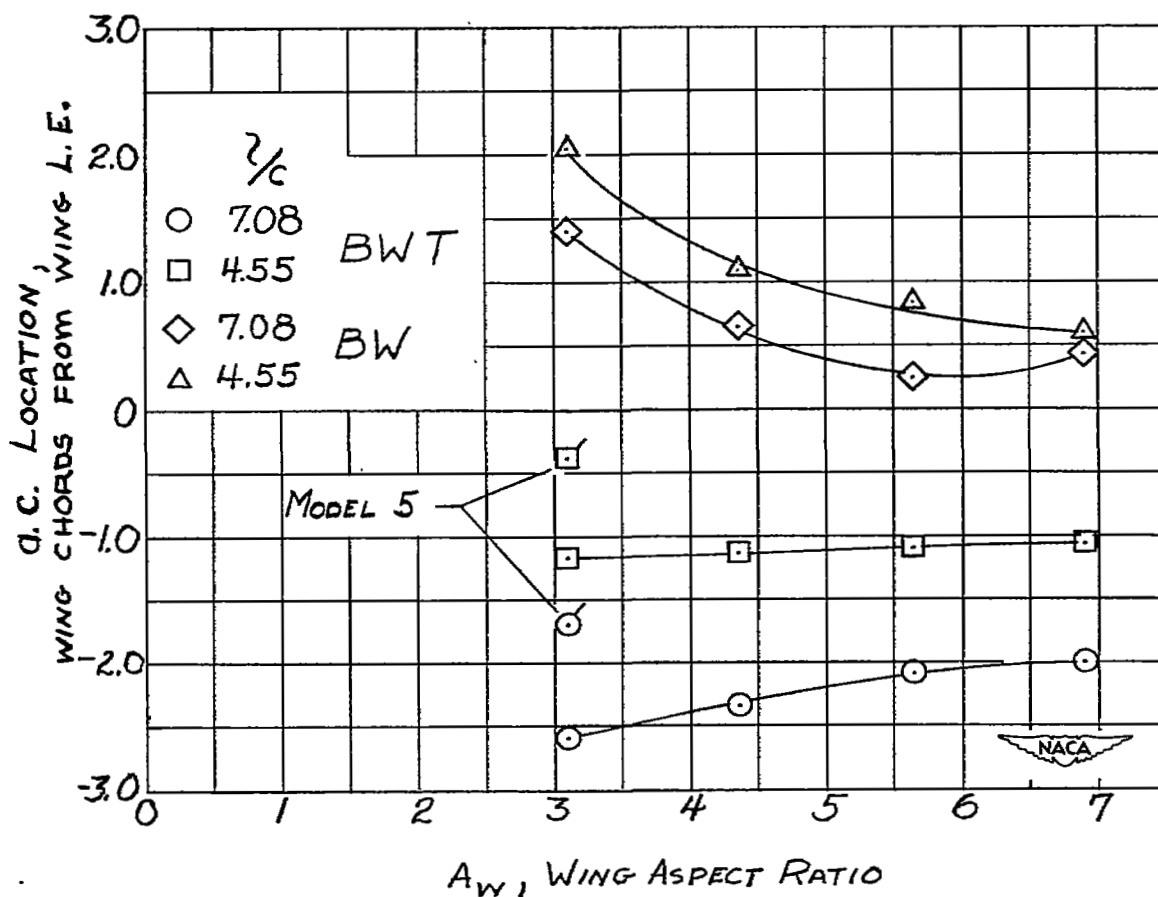


Figure 9.- Variation with wing aspect ratio of the aerodynamic-center location at $\alpha = 2^\circ$ for the BWT and BW configurations. (Positive values ahead of wing leading edge.)

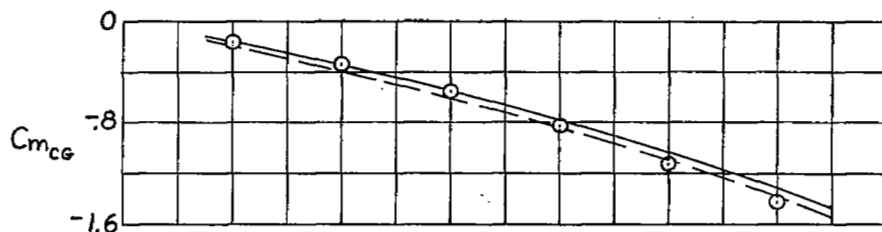
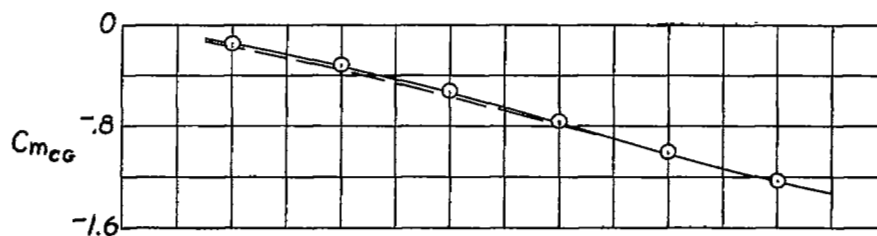
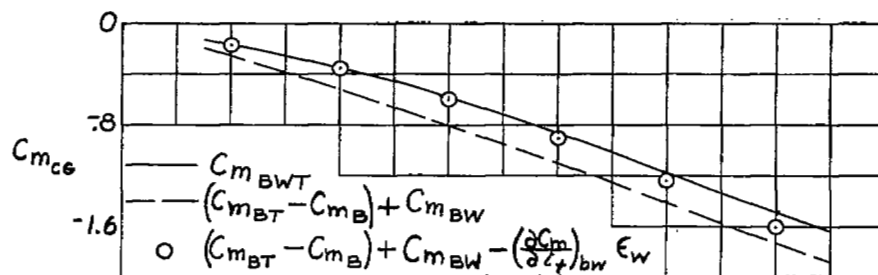
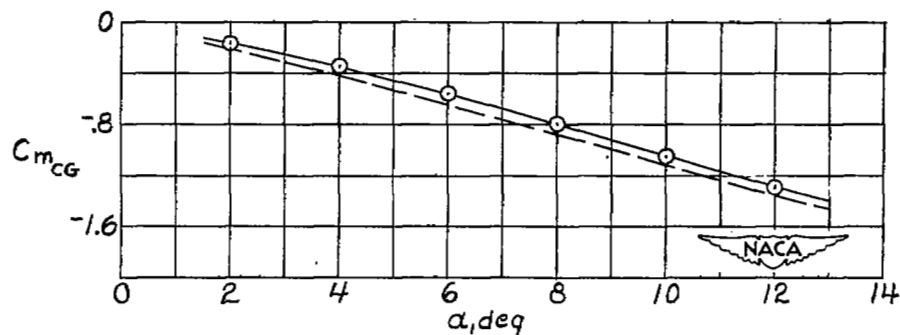
(a) Model 1, $\frac{l}{c} = 7.08$.(b) Model 1, $\frac{l}{c} = 4.55$.(c) Model 2, $\frac{l}{c} = 7.08$.(d) Model 2, $\frac{l}{c} = 4.55$.

Figure 10.- Effect of wing downwash on the pitching moment of the BWT configurations.

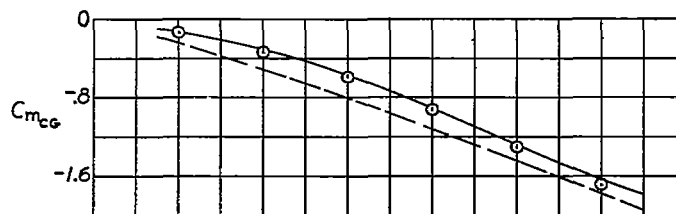
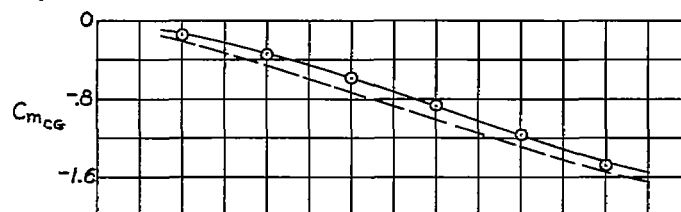
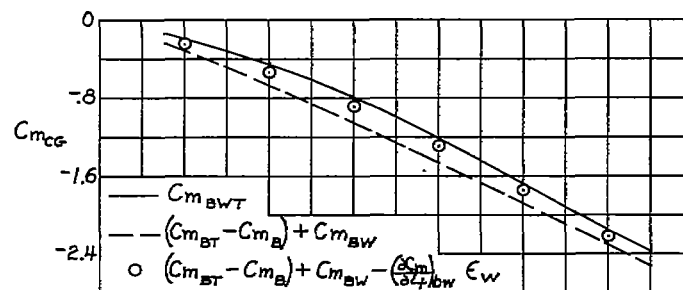
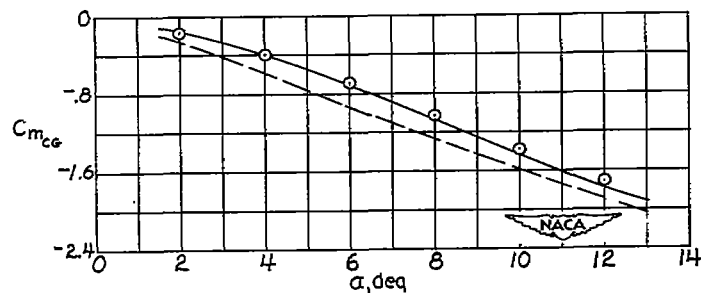
(e) Model 3, $\frac{l}{c} = 7.08$.(f) Model 3, $\frac{l}{c} = 4.55$.(g) Model 4, $\frac{l}{c} = 7.08$.(h) Model 4, $\frac{l}{c} = 4.55$.

Figure 10.- Continued.

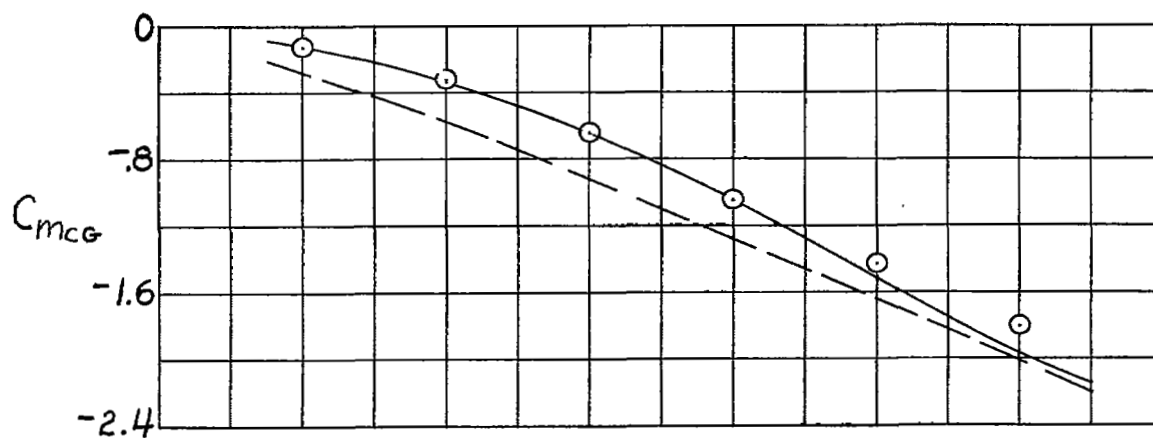
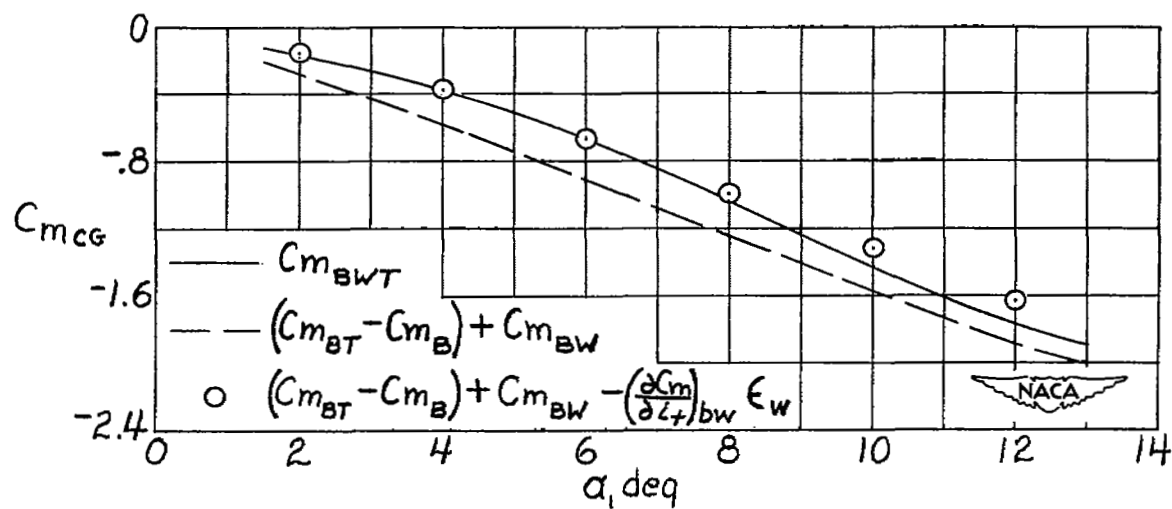
(i) Model 5, $\frac{l}{c} = 7.08$.(j) Model 5, $\frac{l}{c} = 4.55$.

Figure 10.- Concluded.

NASA Technical Library



3 1176 01436 2355